GAS-PHASE EXTRACTION OF GOLD FROM TAILINGS: INSIGHTS FROM DENSITY FUNCTIONAL THEORY AND THE EMPIRICAL

Ibrahim Abdullahi Ali

A dissertation submitted to the Faculty of Engineering and the Built Environment
in partial fulfillment of the requirements for the degree
Master of Science in Engineering

University of the Witwatersrand
Johannesburg
South Africa

March 2021

Declaration

I declare that this dissertation is my own unaided work. It is being submitted for the degree of Master of Science in Engineering to the University of the Witwatersrand, Johannesburg. It has not been submitted before for any other degree or examination at any other university.

Abstract

A process that does not depend on water as a medium for reaction is beneficial in water-strapped regions such as South Africa. This thesis describes such a process. Gas-phase extraction involves a volatile organic reagent that reacts with a metal of interest. In the process under investigation, a volatile organic ligand reacts with solid, native gold transforming it in a gas phase. Studies have shown that β-diketone ligands such as acetylacetone and its derivatives could be used as the volatile ligand in the process. This process is capable of extracting gold from low-grade ores and presents a lower environmental risk than the cyanide process. It also has the added advantage that the extractant can potentially be recycled.

The gold content in the material under investigation was 0.3 g/t Au and the average particle size of the sample was 9 µm. The material falls into 'Group C' of Geldart's classification and cannot be fluidized, owing to its cohesive nature and strong interparticle forces.

A density functional theory (DFT) study on the structure and properties of three Au(III)-β-diketonato complexes: Au(III)-acetylacetonate, Au(III)-trifluoroacetylacetonate and Au(III)-hexafluoroacetylacetonate—is presented. The HOMO-LUMO gap of the Au(III)(β-diketonato)$_3$ complexes have been calculated and were found to be very similar, showing similar stability of the three complexes. Thus, indicating that acetylacetone is as good as any of the two other, more expensive β-diketone ligands in extracting gold. Acetylacetone was therefore used as the extractant in this study. The extraction of gold was measured at temperatures of 190, 210, and 250°C and a bed mass of 20 g. The highest extraction of gold was obtained at 250°C with an extraction efficiency of 50%. SEM-EDS images and XRD of the tailings after the gas-phase extraction showed evidence that the acetylacetone ligand attacks and breaks down the pyrite and the implication is that in time the refractory gold will be extracted.

Acknowledgments

First, I would like to thank Almighty God for giving me the strength to complete this thesis.

Writing a dissertation is such a tedious endeavour and as such I offer immense gratitude to those who constantly encouraged me never to give up. I should like to thank my supervisors, professors Herman Potgieter and Adam Luckos, and Paul den Hoed, for their invaluable guidance, encouragement and supervision. Your constructive comments and patience is greatly appreciated.

My special thanks and appreciation to Professor Jeanet Conradie for her assistance, suggestions and guidance in the DFT section of this thesis.

I would like also to acknowledge and show my deep appreciation for the financial support provided by Professor Herman Potgieter and DRDGOLD Ltd. Without their financial support the successful completion of this dissertation would not have been possible.

Last but not least, I would like to thank my parents and my siblings for their understanding and encouragement during this study.

Publications

Conference paper

I.A. Ali, J.T. Wainer, J.H. Potgieter, and J. Conradie (2021). Value from fine waste: Gas-phase Extraction of Gold from Mine Dumps. In: Worldgold conference 2021. Pp.137-147

Contents

List of Figures

List of Tables

Notation

AAS	Atomic absorption spectroscopy
AMD	Acid mine drainage
ACAC	Acetylacetone
DB18C6	Dibenzo-18-crown-6
DFT	Density functional theory
HFA	Hexafluoroacetylacetone
HOMO	Highest occupied molecular orbital
HPFOA	pentadecafluorooctanoic acid
LUMO	Lowest unoccupied molecular orbital
$Matrix_{solid}$	Unreacted solid
$(Ext)_{gas}$	Metal complex
$(matrix)_{solid}$	Solid matrix containing the metal to be extracted
MO	Molecular orbital theory
Pnaa	bis(pent-2,4-dionato) propan-1,2-diimine
SEM-EDS	Scanning electron microscopy with energy-dispersive spectrometry
SFE	Supercritical fluid extraction
TFA	Trifluoroacetylacetone
XRD	X-ray diffractometry
XRF	XRay fluorescence spectrometry
U_{mf}	Minimum fluidizing velocity
ρ_s	Density of a solid
ρ_g	Density of gas

1 INTRODUCTION

1.1 Background

Gold is a precious metal and used as coinage and jewelry and it is also used in industrial applications as a catalysts. The extraction of gold was done extensively throughout history, owing to its unique physical and chemical properties as well as its huge inherent value (Marsden and House, 2006). South Africa is one of the largest producers of gold. It was the top producer of gold until 2009, when China became the largest gold producer in the world and has since fallen to eighth position after China, Australia, Russia, USA, Canada, Peru and Indonesia (Neingo and Tholana, 2016). However, the extraction and production of gold are still contributing significantly to the South African economy. The mining industry, of which gold is a part, contributed 7.3 % to the South African gross domestic product (GDP) in 2018 (Minerals Council South Africa, 2018).

There are several processes used to extract valuable metals from their ores. The two most common methods are hydrometallurgy and pyrometallurgy. Hydrometallurgy refers to the extraction of metals through aqueous systems (Shamsuddin, 2016). Pyrometallurgy is the extraction of metals at elevated or high temperatures. It is mostly used for high concentrated materials; for example, for high-grade ores (Seetharaman *et al.* 2014). Despite their extensive use in the industry, both processes have their disadvantages. Hydrometallurgy produces large volumes of effluents which need extra treatment and lead to the creation of acid fumes (Chen *et al.* 2011). Pyrometallurgy is an energy-intensive process and leads to the formation of greenhouse gases (Van Dyk *et al.* 2012).

The increasing demand for gold as well as the exhaustion of high-grade ores led to the exploration of low-grade ores. However, the conventional gold extraction techniques (pyrometallurgy and hydrometallurgy) are not effective in recovering gold from low-grade ores, since the gold is refractory in these ores. An ore is said to be refractory when gold particles are locked within other minerals, usually sulfides and silicates. To

extract gold from a refractory ore, pre-treatment is required. These techniques are not economically viable: process and operating costs are high (Mbayo *et al.* 2019).

In addition, Industry is under pressure to lower the emissions of SO_2 and CO_2 and to neutralize before disposal (Seetharaman *et al.* 2014). There is a need to develop technologies that will recover metals from low-grade ores, slags, fly ash and sewage sludge (Chen *et al.* 2011). Gas-phase extraction is an attractive possibility as it yields high recoveries from low-grade ores at elevated temperatures and the reagent can be regenerated (Potgieter *et al.*, 2006). The process involves a volatile organic reagent that reacts selectively with a metal of interest. In the process under investigation a volatile organic ligand reacts with solid, native gold. The product, an organo-metallic complex, is a vapour at elevated temperatures.

In this project, a gas-phase extraction process in a fixed-bed reactor will be used to extract gold from a gold tailing stream.

1.2 Problem statement

Besides jewellery gold is used in many modern-day devices, such as electronic devices and computers. It is also used in finance to stabilise currencies in many parts of the world. However, the decrease in gold resources as well as the huge capital involved in primary gold mining led to the exploration of a non-conventional means of extracting gold from secondary sources such as slags and mine tailings. Slags and tailings from metallurgical processes are usually dumped. In Johannesburg, for example, there are about 350 mine dumps, the residue of gold processing. They cover about 320,000 hectares (Van Rensburg, 2016). The land occupied by the dumps could be used for real estate. The dumps also adversely affect the environment by generating polluted water (AMD) (Potgieter *et al.* 2006). It therefore makes economic and environmental sense to recover gold from these dumps. We propose a gas-phase extraction in a fixed-bed to extract gold from low-grade ore that remains in these dumps. This process is potentially more economical and efficient for the extraction of gold from low-grade ores and is less harmful than cyanide.

1.3 Research aims and objectives

The *aim* of this project is to determine the viability and applicability of gas-phase extraction for the extraction of gold from gold tailings with a volatile ligand.

The specific *objectives* are—

1. To determine physical properties and chemical composition of the tailing material and its fluidizability
2. To test selected β-diketonato ligands for the gas-phase extraction of gold
3. To identify which of the Au (III) acetylacetonate complexes is most stable by DFT
4. To measure the rate of extraction of gold using acetylacetone
5. Determine the kinetics of the gas-phase extraction process
6. To determine the stability of pyrite

Dissertation layout

This thesis consists of five chapters. Chapter one provides motivation for the research and outlines the specific research objectives that will be addressed in the research project. In chapter two, a literature review on the conventional and non-conventional extraction techniques of gold, as well as some literature of beta-diketone ligands, are provided. A literature review on the fluidization of Geldart C particles is also provided. Chapter three describes the experimental procedure followed to conduct the experiments as well as the materials used. In chapter four the experimental results are presented and discussed. In the final chapter, the main conclusions of the research are presented and recommendations are made for future work.

2 LITERATURE REVIEW

2.1 Gold chemistry

Gold is a very stable metal and as such does not react with air and in many aqueous solutions. Gold only dissolves in certain complexing ligands that act as oxidizing agents. Examples of these ligands are cyanides, thiosulfates and halides. These ligands make possible the selective extraction of gold as gold ores are generally present in low grade ores. Gold alongside copper and silver occurs in Group 11 of the periodic table. These metals have similar ionization potentials and electronic structures. However, their redox chemistry is quite different. The chemistry of gold is dictated by its high electronegativity—that is, its affinity for electrons (Marsden and House, 2006).

Gold exists in one of two oxidation states, Au (I) or Au (III). The electron configuration of gold (I) is $5d^{10}6s^{0}$. This configuration indicates a very stable compound and validates the stability of the gold (I) compound. Gold has the lowest electrochemical potential of any metal and as such will readily react with any reducing agent to form metallic gold. The energy difference between the s, p and d orbitals of gold (I) (aurous) is very small, hence the two coordinate complex formation of gold (I). This justifies the linear complex formation of gold (I). Many species that form stable gold complexes are listed in Table 2.1. Some ligands form stable complexes with Au (I) and others with Au (III). The choice of formation is dictated by the oxidation state, e.g., soft donor ligands (*i.e.*, thiourea and cyanide) prefer low valency metal ions (Marsden and House, 2006) and form stable complexes with Au (I). However, hard donor ligands prefer high valency metal ions and such form stable complexes with Au(III).

Table 2. 1: Stability constants (Dimensionless) for selected Au (I) and Au (III) gold complexes adopted from Marsden and House (2006).

Ligand	**Au (I), β_2**	**Au (III), β_3**
CN^-	2×10^{38}	10^{56}
SCN^-	1.3×10^{17}	10^{42}
$S_2O_3^{2-}$	5×10^{28}	$-$
Cl^-	10^9	10^{26}
Br^-	10^{12}	10^{32}
I^-	4×10^{19}	5×10^{47}
$CS(NH_2)^{2+}$	2×10^{23}	$-$

Where β_2 and β_3 are the stability constants of Au (I) and Au (II) respectively.

2.2 Gold tailings

Gold tailings are the residues left over and dumped in slime dams after separating and recovering gold. In South Africa gold tailings refers to the tailings of cyanidation extraction process. In Johannesburg there are about 350 gold mining dumps that cover large tracts of land. The high prices that gold and land fetch have driven to the exploitation of these gold tailings and reprocessing them to recover economic value from minerals and land (Van Rensburg, 2016). About 1.7 billion tons of gold tailings have been produced in South Africa from which 15 million ounces of gold can be recovered (Ogola *et al.,* 2018). Reprocessing of these tailings also has the added advantage that it will minimize environmental problems related to mine dumps, e.g., acid mine drainage (AMD). The oxidation of pyrite (FeS_2) in the presence of water and oxygen leads to AMD. The overall effect of this reaction is that it lowers the pH by releasing H^+ ions and therefore retaining the solubility of the ferric ion. The tailings used in this research are from the plant run by Ergo Mining Proprietary Limited (Ergo), a reclamation operation owned and managed by DRDGOLD Limited. DRDGOLD is a gold-producing company that specializes in surface tailings retreatment. It treats between 2 and 2.1 Mt of gold-bearing tailings a month (DRDGOLD 2017, Annual Integrated report). The Ergo plant in Brakpan, 50 km east

of Johannesburg, has a gold grade of about 0.32 g/t, and about 60% of the gold is recovered at the plant. This leaves unprocessed gold of about 0.1–0.15 g/t (DRDGOLD, 2017).

The feed to the Ergo plant is drawn from three sources: (1) surface tailings (2) slime dams, and (3) sand dumps. These feeds are left over from mining operations done at the Witwatersrand basin in Johannesburg. Sand dumps are the result of the stamp milling process. This is an inefficient process used in old mining operations. Sand dumps contain large quantities of gold, however, the gold is captured in coarser grain particles. Slime dams are also the result of old mining operations containing lower grades of gold. In Figure 2.1 a DRDGOLD tailings map is provided. The map shows the location of the dumps as well as the deposition of their process tailings.

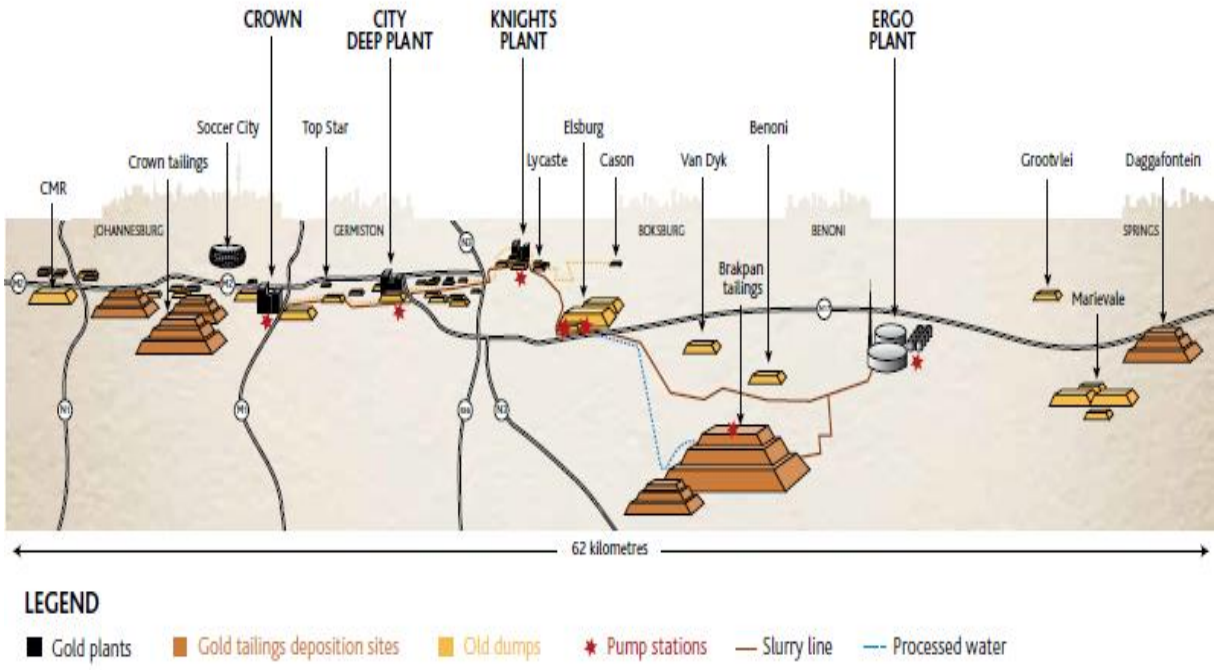

Figure 2. 1 : DRDGOLD Limited tailings map (DRDGOLD, 2017)

The DRDGOLD ore is refractory since most of the gold particles are locked within other minerals, such as sulfide and silicates. The different forms that gold is associated with in sulfidic minerals is shown in Figure 2.2. Gold can be found as free-milling (readily liberated) with in the mineral, along the grain boundaries, at the boundary between sulfide grains, gold enclosed within the pyrite, along fractures and/or crystal defects and as a colloidal particle in solid solution in the sulfide. The free milling gold ores are amenable to cyanidation and high gold recoveries can be achieved (Marsden & House, 2006). However, in cases where the gold is locked in the sulfide minerals, cyanidation does not achieve high gold recoveries since the sulfide minerals provide sulfide ions which interfere with the cyanidation reaction by forming insoluble species on the gold grain surfaces (Coetzee *et al.* 2011).

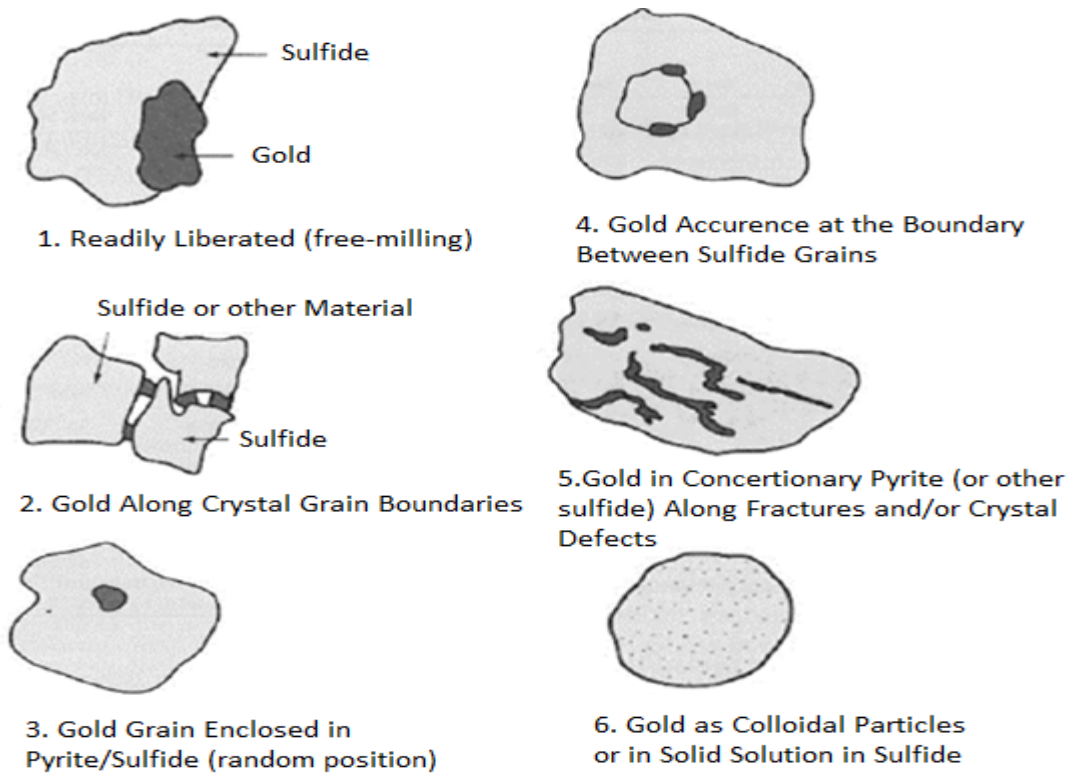

Figure 2. 2 : Different forms in which gold is found within sulfidic minerals (Marsden & House, 2006)

2.3 Extractive metallurgy of metals by conventional methods

Extractive metallurgy deals with the extraction of valuable metals from an ore. The metals are present in an ore as sulfides or oxides and normally must be reduced physically, chemically or electrolytically to convert them into a pure metal.

The method of extraction of gold from its ore depends on the state in which the gold is found. Gold ores fall into three categories: (1) placer, (2) free-milling, and (3) refractory (La Brooy *et al.* 1994).

In placer ores, gold is found freely and can easily be recovered by direct amalgamation. In free-milling ores, the ore must first be ground to free gold particles before extraction. In refractory ores, the gold particles are encapsulated in a host mineral. Refractory ores can be either sulfidic, carbonaceous and/or telluric (Gupta and Mukherjee, 1990).

Metals are traditionally extracted from their ores by a pyrometallurgical, hydro-metallurgical or electrometallurgical route.

2.3.1 Hydrometallurgy

Hydrometallurgy involves the extraction of metals and their production through aqueous solutions (Shamsuddin, 2016). Hydrometallurgy is the most recent technique compared to pyrometallurgy and has the potential advantage of high selectivity and can be used to extract metals from low-grade ores (Seetharaman *et al.* 2014). However, despite its selectivity, the hydrometallurgical route has two major disadvantages: (1) the extraction rate is slower at room temperatures than in a commensurate pyrometallurgical route, and (2) the process produces large volumes of effluent that need extra treatment and could potentially pollute groundwater (Chen *et al.* 2011).

In hydrometallurgy, there are two steps taken to obtain the metal value. The first step involves bringing the metal into aqueous solution and is known as leaching or lixiviation. In the second step, the leach liquor is cemented or precipitated to recover the metal of interest (Shamsuddin, 2016). The cyanidation process is the preferred

method of leaching in the gold extraction. Gold easily dissolves as $[Au(CN)_2]^-$ in dilute cyanide solutions. Habashi.(1967) suggested that the reaction of gold with cyanide is electrochemical in nature and takes place in the presence of oxygen as shown in Eq. (2.1):

$$2Au + 4NaCN + O_2 + 2H_2O \rightarrow 2NaAu(CN)_2 + 2NaOH + H_2O_2 \quad (2.1)$$

The rate of dissolution of gold is dependent on the concentration of the cyanide, temperature, pH, and the partial pressure of oxygen (Shamsuddin, 2016). This cyanidation process (Eq. 2.1) has been the leaching method of choice for many decades. However, there are environmental concerns associated with cyanide leaching. Cyanide leakage from tailing storage areas could have a devastating impact on the surrounding environment. High concentrations of cyanide can pose serious health effects to many living organisms (Hilson and Monhemius, 2006).

2.3.2 Pyrometallurgy

Pyrometallurgy is the extraction of metals at high temperatures, often in the presence of a reductant. There are several processes involved in pyrometallurgy: these processes are roasting, smelting and refining. Roasting is the application of hot air to an ore, and it is usually applied to sulfide minerals. During the process, the sulphide mineral goes through oxidation and this leads to the formation of sulfur dioxide gas and solid metal oxide. In smelting, heat and a reducing agent is used to obtain a base metal from an ore. The most common reducing agent used is carbon which reacts with oxygen forming CO and CO_2, leaving behind the metal base. Refining refers to the purification and increasing the grade of the metal. In pyrometallurgy it is important to know the melting and boiling points of the metal of interest and its alloys. For example, gold melts at 1064°C and boils at 2808˚C under atmospheric conditions (Marsden and House, 2006). The downside of pyrometallurgy compared to other metallurgical processes is that it requires much more energy and high capital expenditure (Shamsuddin, 2016).

2.3.3 Electrometallurgy

Electrometallurgy is the extraction of metals by making use of electrical energy. Electrometallurgy is usually headed by hydrometallurgy or pyrometallurgy and serves as the recovery process in metal production (Shamsuddin, 2016). The two main processes involved in electrometallurgy are electrowinning and electrorefining. Electrowinning refers to the electrodeposition of metals from an electrolyte solution (pregnant solution) which is obtained from leaching (Shamsuddin, 2016). Electrorefining involves the removal of impurities from the metal and uses a similar process to that of electrowinning (Wai *et al,* 2009).

2.4 Non-conventional methods of extracting gold

Owing to problems associated with conventional methods of extracting metals, extensive research has sought to develop alternative technologies. These new technologies include supercritical fluid extraction and gas-phase extraction.

2.4.1 Supercritical fluid extraction of metals

A supercritical fluid is any material that is above its critical point in pressure and temperature. It displays the mass transfer characteristics of a gas and dissolving characteristics of a liquid, therefore exhibiting gas and liquid behaviour at the same time. The most used supercritical fluid is carbon dioxide (CO_2). It has been chosen, because of its low critical temperature and pressure, low toxicity and because it is cheaper than other fluids (Turner *et al.* 2002).

The linear structure of CO_2 validates its non-polar nature and its affinity for non-polar compounds. Supercritical fluid extraction (SFE) has replaced traditional solvent extraction of organic compounds, because SFE is relatively fast and its selectivity can easily be tuned for an intended purpose (Chen *et al.* 2011). Extraction of metal ions by only supercritical CO_2 ($scCO_2$) is highly ineffective due to weak solute-solvent contact and charge neutrality necessity. However, the solubility of metal ions in ($scCO_2$) can be increased by chelating them with organic ligands.

Bai and Yang (2006) extracted various metal ions using bipyridine derivatives as the chelating reagent in a $scCO_2$. The metals extracted were divalent metal ions of cobalt (Co), copper (Cu), cadmium (Cd), zinc (Zn), lead (Pb) and strontium (Sr). The metal ions were extracted from spiked filter paper with extraction extents of 100% (Co^{2+}, Cu^{2+}, Zn^{2+}), (100%), 98% (Cd^{2+}), 90% (Pb^{2+}), and 79% (Sr^{2+}). Although the extraction extents are high, when the recovery of a mixed metal ions was measured, extraction had no selectivity for the metal ions.

Mochizuki *et al.* (1999) investigated the supercritical extraction of alkali metal ions from aqueous solutions of potassium and sodium using crown ether as the complexing ligand. They found that their extraction of the alkali metal ions increased when they combined the crown ether with pentadecafluorooctanoic acid (HPFOA). This is because the HPFOA supplies CO_2-philic counter ion for the metal ligand complex and has a synergistic effect in the process. Similarly, Leybros *et al.* (2016) studied the feasibility of $scCO_2$ as a decontamination method for contaminated soils with non-radioactive cesium as the contaminant by making use of synergistic leaching. They used a mixture of Dibenzo-18-crown-6 (DB18C6) crown ether with HPFOA and managed to extract up to 95% of the cesium from the soil.

2.4.2 Gas-phase extraction

Gas-phase extraction is a technique that can be applied to the extraction of heavy metals in low-grade ores such as soil, sediments, and used catalysts. It involves a volatile organic reagent that selectively reacts with the metal of interest (Potgieter *et al.* 2006). The following reaction describes the extraction (Chen *et al.* 2011):

$$Ext_{\text{gas}} + M(Matrix)_{\text{solid}} \rightarrow M(Ext)_{\text{gas}} + Matrix_{\text{solid}} \quad (2.2)$$

Where *Ext* denotes an extractant, *M* denotes the metal (gold in this instance), *Matrix* denotes the source of the metal (tailings).

A carrier gas removes the volatile metal complexes resulting from the reaction. A flow sheet of the extraction method as proposed by Allimann-Lecourt *et al*. (2002) and Chen *et al.* (2011) is shown in Figure 2.3.

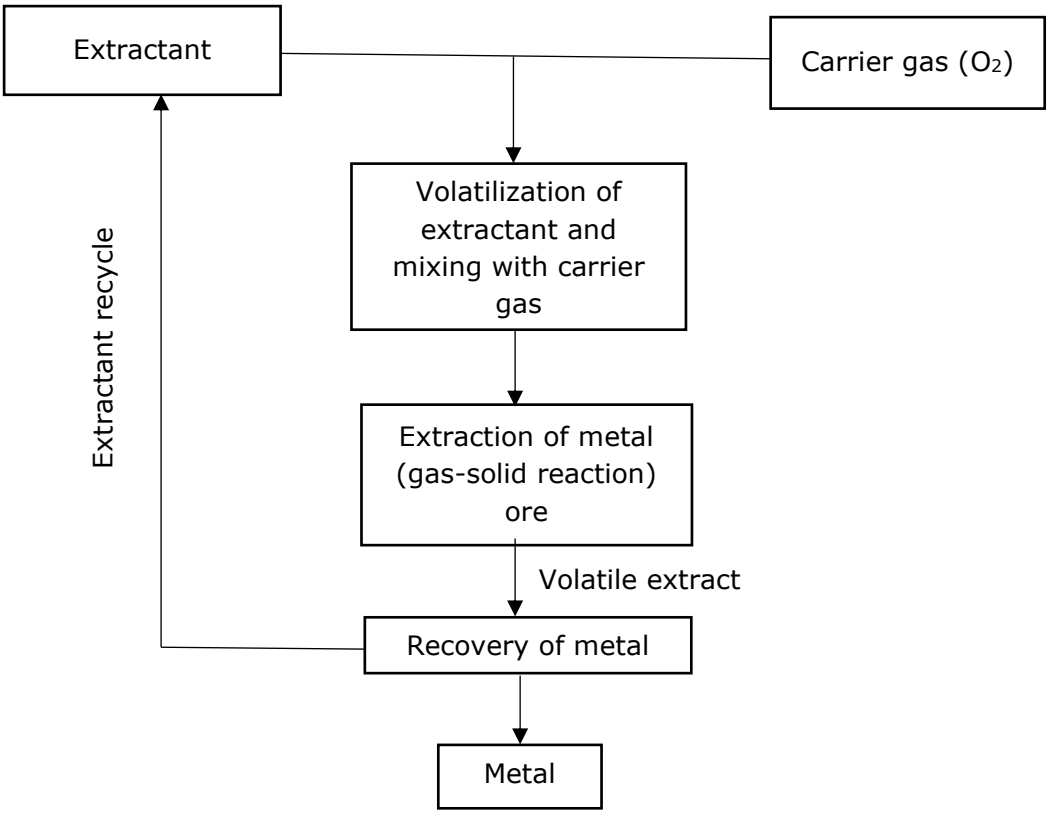

Figure 2. 3 : Flow sheet of gas-phase extraction

A volatile organic ligand reacts with solid, native metal and carries it away in a gas phase. The type of volatile ligands used to date are mostly β-diketones and their derivatives. The two carbonyl groups in β-diketones are divided by a single carbon atom. β-diketones can be used as a chelating agent: the organic molecule accommodates the metal in one of three ways, denoted as type 1, 2, and 3 (see Figure 2.4; Pettinari and Santini, 2016).

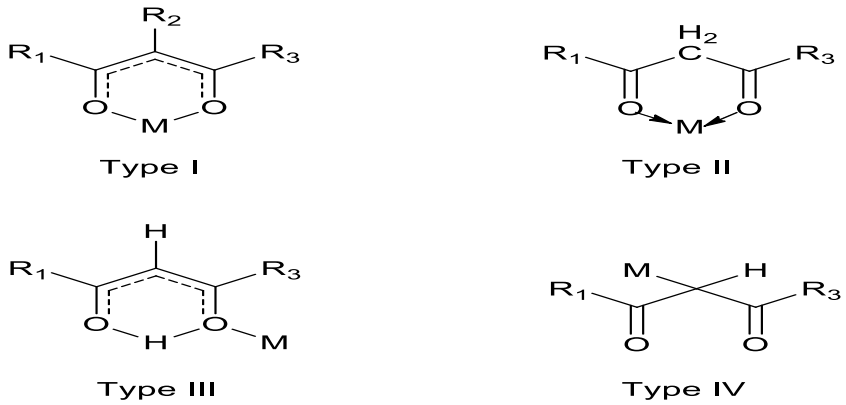

Figure 2. 4 : Coordination modes of β-diketone ligands (Pettinari and Santini, 2016)

In most β-diketones the alpha carbon has a hydrogen as a substituent, but the substituents can be an alkyl group, fluorinated alkyl group or a hetero-aromatic group (Haas and Franz, 2009). The simplest and most common diketone is acetylacetone.

Allimann-Lecourt *et al.* (2002) employed the SERVO process to extract various metals from fly ashes using β-diketones, β-diketoimines and tetra-alkyldithphosphoramides. They used specifically acetylacetone, bis-(pentane-2,4-dionato) propan-1,2-diimine (pnaa) and tetra-iso-propyldithiophosphoramide (prps). The SERVO process uses a volatile chelating agent which is selective towards the metal of interest in extracting heavy metals. They extracted 82% and 80% of nickel and vanadium respectively using prps, while pnaa yielded 43% and 23% respectively, and acac could achieve 64% and 15% recovery, respectively.

Potgieter *et al. (*2006) assessed the practicality of using gas-phase extraction in a fluidized bed to extract metals from solid oxides with acac. Table 2.2 summarizes their findings in part.

Table 2. 2: Optimum conditions for the recovery of various metals using gas-phase extraction with acac

Metal	Temperature [˚C]	Time [min]	Recovery [%]	Activation energy [kJ/mol]	Type of reaction control
Aluminium (Al)	190	105	64	28	Surface reaction
Chromium (Cr)	210	150	48	23	Surface reaction
Vanadium (V)	190	120	63	5	Diffusion control
Iron (Fe)	180	45	75	181	Chemical reaction

The percentage of iron was the highest (75%), whereas extraction was the lowest for chromium (48%). Although the energy required to start the reaction was higher for iron, the highest percentage of recovery was achieved for iron in the shortest time.

Similarly, Van Dyk *et al.* (2012) studied the extraction of iron and lead from synthetic hematite (Fe_2O_3) and synthetic massicot (PbO) using gas-phase extraction in a fluidized bed. They recovered 87% of iron and 88% of the lead from 1 mass % of their respective oxides with acac. The reaction lasted for 4 hours at a temperature of 250°C and an acteylacetone flow rate of 1 mL/min for iron, while for lead the acetyleacetone flow rate was 3 mL/min. Furthermore, Machiba (2020) extracted gold from tailings using acetylacetone in a gas-phase, he extracted 65% of the gold at 250°C.

The extraction of metals using gas-phase extraction is feasible for various metals as shown above. This investigation will focus on the extraction of gold from tailings using gas-phase extraction in a fixed bed reactor.

2.5 Fluidization

2.5.1 Particle size and fluidization characteristics

Fluidization depends on the size, the shape, and the density of the particles (Leion *et al.* 2018). Geldart (1973) studied the behaviour of solid-gas fluidization and classified them according to the density difference ($\rho_s - \rho_g$) and mean particle size into four distinct groups; he developed a chart now known as the Geldart Particle Classification Diagram (see Figure 2.5).

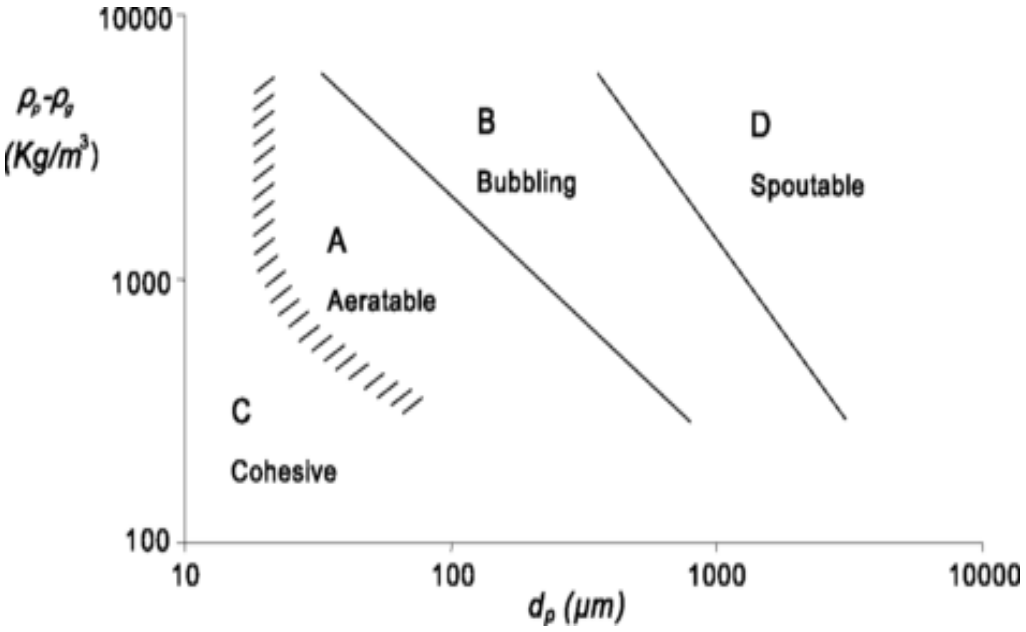

Figure 2. 5 : Geldart classification chart (Geldart 1973)

Group A: These powders have particles sizes between 30-100 μm and low particle densities (less than 4 g/cm^3). The inter-particle forces between these powders are not as great as those in group C, and these particles fluidize well, with fluidization possible at low gas flow rates. Fluid catalytic cracking (FCC) catalyst is an example of such particles.

Group B: These particles generally have particles sizes between 40–500 μm and their density is between 1.4–4.0 g/cm^3. These are sand like particles and unlike group A particles, bubbles form at velocities higher than the minimum fluidization velocity (U_{mf}). Table salt is a representative of these types of solids.

Group C: These particles are very cohesive and are fine sized (powders). Group C particles generally have sizes less than 30 μm. Normal fluidization is tremendously difficult for these powders because inter-particle forces are larger than those caused by the action of the gas.

Group D: These are the largest of Geldart group particles. They are spoutable solids and difficult to fluidize. Gasification of coal and drying of grains are some examples of processes where these types of solids are used.

2.5.2 Fluidization of fine particles

The fluidization of fine particles (Geldart C particles) is extremely difficult, owing to the cohesive nature and the strong interparticle forces between these powders. These powders are of interest, because of their large surface-to-volume ratio and the small particle size. They have applications in industry as sorbents and catalysts. When trying to fluidize group C particles, one observes channelling and agglomeration. Channeling is a phenomena observed in the fluidization of cohesive particles where the gas flow has trouble in fluidizing the bed due to the cohesive nature and the strong interparticle force between the powders. The up-flowing gas leads to the creation of vertical voids in the bed (Raganati *et al.* 2018). These voids are called channels and may span the length from the distributor to the bed surface (Han, 2015). This channeling leads to the de-fluidization of the bed.

Cohesive particles can be found in three states in a fluidized bed: Natural agglomerates, newly produced (un-agglomerated) and fluidized agglomerate (Pacek and Nienow, 1990). Geldart type C particles have a tendency to form clusters when stored in a container or when they are transported due to the cohesiveness of these particles, hence the term natural agglomerates (Han, 2015; Raganati *et al.* 2018). To limit the agglomeration and channeling effect of group C powders fluidization aids are needed. These fluidization aids can be in the form of extra energy to break down agglomerates by mechanically stirring or vibrating the system or magnetic and electrical field disturbances. Coarse particles, such as Geldart type B particles can also be added into the bed to aid the flow of the particles and reduce the interparticle forces

between the powders. This technique has advantages over the other methods since there is no necessity for additional apparatus or change in column design (Raganati *et al.* 2018). Ajbar *et al.* (2011) found that they could achieve smooth fluidization of nanoparticles by adding coarse group A type particles (sand) to the bed.

For gas-phase extraction to work effectively, the particles that host the gold would need to make intimate contact with the ligand. A fluidized bed would therefore be an ideal reactor for this process.

However, the density (3.15 g/cm^3) and mean particle size (9 μm) place the tailing material in Group C of Geldart's classification of fluidization types. Beds of Group C particles do not fluidize or are difficult to fluidize.

2.6 Coordination chemistry of β-diketones and their derivatives

Coordination chemistry deals with the structure of molecules that possess a central atom (mostly metallic) attached to an electron-donating molecule (ligand). The ligand acts as a Lewis base by donating one or more of its electron pairs to the metal. β-diketones and Schiff base ligands are considered in this research.

Acetyleacetone is a β-diketone ligand. It exists in a tautomeric keto and enol form (see Figure 2.6).

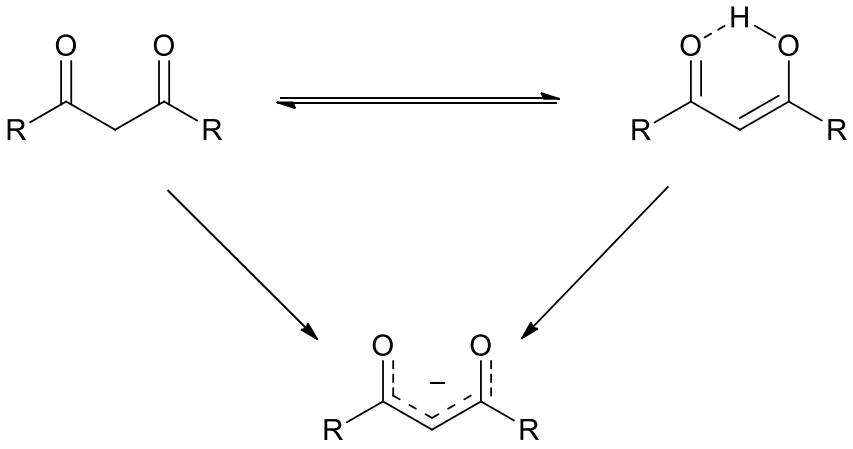

Figure 2. 6 : β-diketone tautomerization

β-diketones are easily deprotonated—*i.e.,* hydrogen on the α-carbon is removed—by strong bases. The acidity of the β-diketone is dictated by the nature of substituents. Electron-withdrawing groups increase acidity, whereas electron-donating groups decrease acidity (Haas and Franz, 2009). Perfluorinated alkyl group substituents increase Lewis acidity. β-diketones with an aromatic moiety have stronger light absorption than their aliphatic derivatives. Dibenzoylmethane (DBM) absorbs UV radiation and is utilized in the cosmetic industry as sunscreens (Zawadiak and Mrzyczek, 2012).

Metal-acetylacetonates are usually prepared from the reaction of acetylacetone with a metallic element. They are used as catalysts in significant organic reactions such as polymerization, oligomerization, hydrogenation and isomerization of olefins. The β-diketones can bind to metals in many different ways. However, the acac anion generally forms a bidentate complex with metals by binding through the two oxygen atoms. The negative charge of the acetylacetonate ligand is delocalized and leads to the formation of six-membered chelate rings upon encountering a metal (see Figure 2.7).

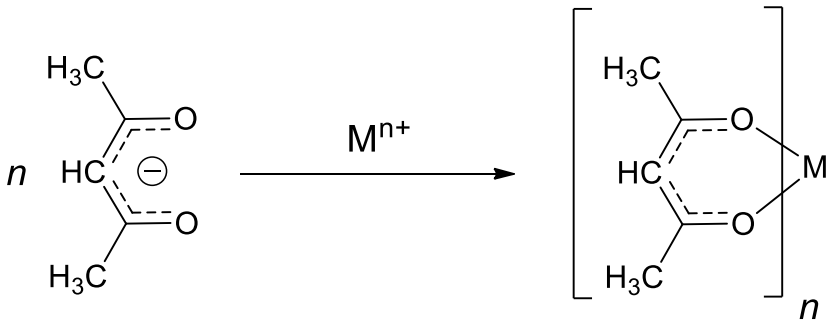

Figure 2. 7 : Acetylacetonate complex with a metal

A base can be added to the reaction to shift the equilibrium and favour the formation of the complex. However, in most cases the chelating effect is so strong that no added base is required to form the complex. The complex can be reduced from the (condensed) gas phase to obtain a metal product and the reagent can be regenerated

and recycled. The choice of ligand depends on the ease of volatilization and the stability of the volatile complex formed. Potgieter *et al.* (2006) tested the feasibility of using β-diketones for the gas-phase extraction of different metals in their solid oxides. With acetylacetone they extracted 75% of iron and 48% of chromium.

2.6.1 Schiff Bases

A Schiff base is the nitrogen equivalent of an aldehyde or ketone in which the C=O moiety is replaced by a C=N-R group. It is usually synthesized from an aldehyde or ketone in the presence of primary amine by condensation (see Figure 2.8):

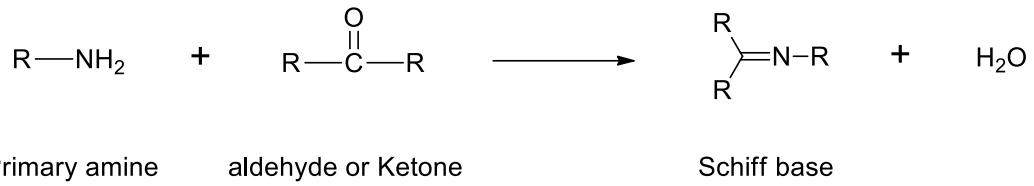

Figure 2. 8 : Schiff base formation (Xavier and Srividhya, 2014)

The basicity of the imine nitrogen and its pi-acceptor abilities make Schiff bases common ligands in coordination chemistry. Schiff bases have been used in synthetic chemistry and are intermediates to many enzymatic reactions. They facilitate the interaction between the amino/carbonyl group of the substrate with an enzyme. Allimann-Lecourt *et al.* (2002) prepared various Schiff bases for the SERVO process to extract transition metals. Amongst the ligands prepared was bis(pent-2,4-dionato) propan-1,2-diimine (pnaa), which was found to be suitable for divalent metals and selectively extracted nickel from fly ash.

2.7 Density functional theory

Density functional theory (DFT) is a technique used to calculate molecular structure of compounds. It provides qualitative and quantitative information on the ground state properties of a molecule (Atkins and De Paula, 2010). It is faster than the ab-initio computational quantum modelling techniques such as Hartree-Fock. Depending on

the application, the values obtained in DFT are in good agreement with the experimental values. Computer modelling makes use of numerical models to study the properties and structure of molecules. These computer modeling techniques can be ab-initio, DFT, or semi-empirical techniques. The former of the two methods makes use of the numerical solution of the Schrödinger equation, whereas the latter is based on approximate or effective functions to determine the force between the particles (Shriver *et al.* 2010).

DFT developed in the 1960s when Kohn and Sham proposed their equations shown in Equation 2.3. Since then the technological advances in the computer industry led to the use of DFT in chemistry, solid state physics, biology and material sciences (Qi *et al.* 2016)

$$\left\{h_1 + j_0 \int \frac{\rho(2)}{r_{12}} d\tau_2 + V_{XC}(1)\right\} \varphi_m(1) = \varepsilon_m \varphi_m(1) \qquad \text{Kohn-Sham equations [2.3]}$$

In equation 2.3 the first term on the left represents the kinetic and potential energy contribution for one electron, the second term represents the potential energy of repulsion between electrons 1 and 2 while the third term is the exchange correlation potential (V_{XC}) (Atkins and De Paula, 2010).

Density functional theory is centered around the electron density (ρ), rather than the wave function (φ). The energy of the molecules is a function of the electron density and the density is a function of the position, $\rho(r)$. This can be written as:

$$\rho(r) = \sum_m |\varphi_m(r)|^2 \qquad \text{Electron probability density [2.4]}$$

The electron density is constructed from the occupied orbital and is calculated from Kohn-Sham equations (equation 2.3). These equations are very similar to the Hartree-Fock method except for an exchange correlation potential (V_{XC}).

DFT calculations of metal complexes can provide information on the geometry of the complex, electron spectroscopy, thermodynamics and non-covalent interactions. Tayyari *et al.* (2007) carried out DFT calculations on three β-diketones. The β-diketones studied were dibenzoylmethane (DBM), benzoylacetone (BA) and acetylacetone (ACAC). In their studies they investigated the molecular structure and stability,

vibrational frequencies and the hydrogen bond strengths of the three ligands. Their DFT calculations have shown that DBM has a stronger hydrogen between the enol hydrogen and the keto oxygen bond than BA and AA. Similarly, Conradie *et al.* (2015) carried out theoretical (DFT) and experimental studies (Cyclic Voltammetry) on a series of β-diketonato iron(III) complexes. They found that there is a relationship between the reduction of the iron(III) β-diketonato complex and the electron donating abilities of the side groups R_1 and R_2 on the β-diketonato ligand $(R_1COCHCOR_2)^-$. The ease of reducing the complex increases with the electron withdrawing ability of the side groups. The more acidic the side groups are the more electron density that is withdrawn from the metal center. Their experimental values were also in agreement with energies obtained in DFT modelling.

Conradie *et al.* (2019) carried out an electrochemical and computational study of β-diketone ligands. They investigated the effect of aromaticity, electron donating and ester groups on positions 1 and 3 of the β-diketone on the reduction potential. Using DFT and the spin density profile of the reduced β-diketone, they identified the reduction centre. They also found that the lowest unoccupied molecular orbital energy (E_{LUMO}) of the β-diketone is directly related to the reduction potential obtained experimentally. Their findings were significant as these results could be used to predict the expected experimental reduction potential of newly designed β-diketone.

2.8 Summary

This research aims to extract gold from a tailing material. The chapter starts with discussing some basic chemistry of gold as well as the source of the tailings material used in the project. Conventional as well as non-conventional methods of extracting gold are presented. The conventional methods of extracting gold are hydrometallurgy, pyrometallurgy and electrometallurgy. The difficulties associated with extracting gold by these conventional methods are also briefly discussed. The non-conventional methods presented in the literature are supercritical fluid extraction of metals and gas-phase extraction. In gas-phase extraction volatile organic ligand reacts with solid, native gold transferring it to a gas phase. Studies have shown that β-diketone ligands

such as acetylacetone and its derivatives can be used as the volatile ligand in the process. No work has been published to date, however, on the extraction of gold by gas-phase extraction. Hence, the focus of this investigation on the gas-phase extraction of gold. Tailings are a potential commercial application.

3 MATERIALS AND REAGENTS

A refractory gold tailing was used for the experiment. The tailing was obtained from the DRDGOLD plant (The Ergo plant), in South Africa. The volatile organic reagents used and their properties are listed in Table 3.1. All of the reagents were purchased from Sigma-Aldrich.

Table 3. 1: Properties of the various reagents used

Compound	Appearance	Boiling point (˚C)	Purity
Acetylacetone ($C_5H_8O_2$)	Colourless Liquid	140.4	99
1,1,1-Trifluoropentane-2,4-dione ($C_5H_4F_3O_2$)	Colourless liquid	107	99
Hexafluoroacetylacetone ($C_5H_2F_6O_2$)	Colourless liquid	71	99

3.1 Characterization of the tailing material

The physical properties of the tailings were determined using the following analytical techniques: X-ray diffractometry (XRD), X-ray fluorescence spectrometry (XRF), laser diffraction and scanning electron microscopy with energy-dispersive spectrometry

(SEM-EDS) and helium pycnometry. X-ray diffraction (XRD) and X-ray fluorescence (XRF) were used to quantify the chemical and crystalline composition of the particles. Laser diffraction was used to determine the particle size distribution of the tailings. SEM provided information on the surface area characterization of the particles. The helium pycnometer was used to determine the density of the particles.

Table 3. 2:Mineralogy of tailings from DRD

Mineral	Chemical formula	Mass%
Quartz	SiO_2	81.80
Muscovite	$KAl_2(Si_3Al)O_{10}(OH,F)_2$	5.00
Chlorite	$(Mg,Fe^{2+})_5AlSi_3Al_2O_{10}(OH)_8$	3.78
Pyrite	FeS_2	3.06
Pyrophyllite	$Al_2Si_4O_{10}(OH)_2$	2.36
Goethite	$Fe^{3+}O(OH)$	1.74
Rutile	TiO_2	0.61
K-feldspar	$KAlSi_3O_8$	0.41
Biotite	$K(Mg,Fe^{2+})_3[AlSi_3O_{10}(OH,F)_2$	0.34
Diopside	$CaMgSi_2O_6$	0.18
Plagioclase	$(Na,Ca)(Si,Al)_4O_8$	0.44
Other sulfides		<0.10
Other silicates		<0.10
Other		0.17
Total		100

"Other sulfides" include galena, sphalerite and arsenopyrite. "Other" includes tintanite, apatite, monazite, dolomite, calcite and garnet.

3.1.1 X-ray diffractometry

XRD of the tailings was run to quantify the mineral-chemical composition of the sample (see Figure 3.1). Gold associates differently in these minerals. Quartz is the predominant mineral as shown in the diffractogram, and gold locked in silicates is generally difficult to access.

Table 3. 3:Relative abundancies of various minerals in the tailing from DRD

	Compound Name	Formula	Relative Abundance
□	Quartz	SiO_2	Predominant
□	Chlorite	$(Mg,Fe)_6(Si,Al)_4O_{10}(OH)_8$	Minor
□	Muscovite	$KAl_2(Si_3Al)O_{10}(OH,F)_2$	Minor
□	Pyrite	FeS_2	Trace
□	Pyrophyllite	$Al_2Si_4O_{10}(OH)_2$	Trace
□	Microcline	$KAlSi_3O_8$	Trace

Predominant (>50 mass%), major (20–50%), minor (5–20%), trace (<5%)

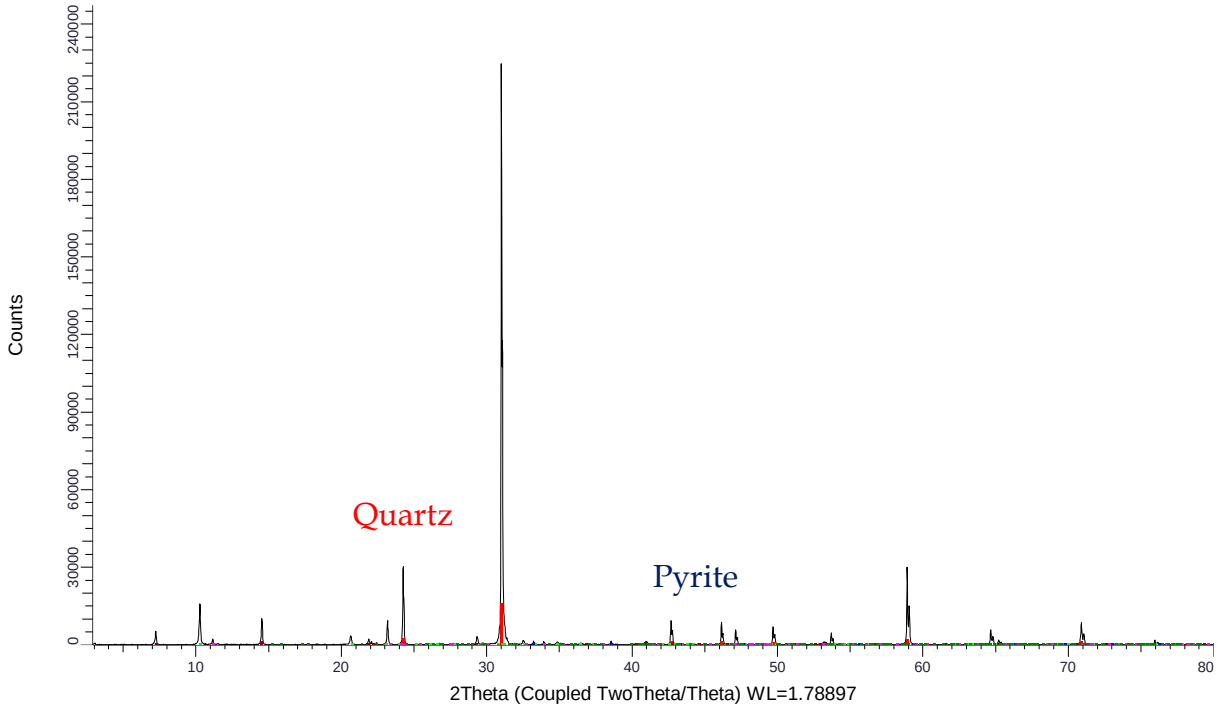

Figure 3. 1: X-ray diffractogram of the various minerals present in the tailings

As mentioned in Chapter 1, the gold ore is refractory since the fine gold particles are encapsulated in other minerals like quartz and sulfides. In the tailings, sulfidic minerals are present in significant amounts as shown in Figure 3.1. These sulfidic minerals are impervious and encapsulate the gold.

3.2 Mineralogy of the DRDGOLD ore

The gold is associated with pyrite (FeS_2, which imparts the refractory character on the gold). To find the gold more readily, a pyrite concentrate was produced by subjecting a sample of Au tailings to heavy liquid density separation. The sulfide reported to the sinks. The concentrate was examined by image analysis (QEMSCAN) by Mintek (Dworzanowski, 2018). The following properties were measured: gold speciation, grain size, liberation of gold and its association with other minerals

A significant fraction of gold—a quarter to a third in the concentrate—occurs in electrum, an alloy of gold and silver (see Figure 3.2). The presence of the electrum

causes the tarnishing of the silver which could lead to poor gold extraction (Zhou and Cabri, 2004).

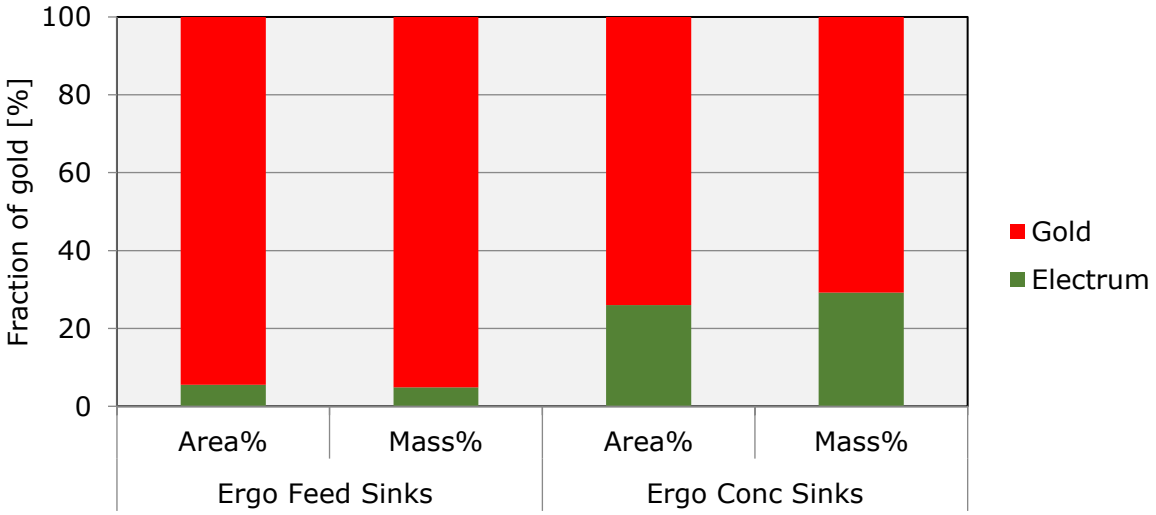

Figure 3. 2: Gold speciation in feed sinks and concentrated sinks

Liberation is defined from two perspectives. One of them is defined by grade: it relates the volume of gold in a particle to the volume of the particle. By this measure, the closer the two volumes are, the more liberated (i.e., measured as a higher percentage) the gold is. This measure is directly applicable to operations in mineral processing (which produces concentrates). The second perspective focuses on the interfacial boundary of gold grains. The measure of liberation is now the fraction of this interfacial boundary that is free (i.e., not adjacent to other minerals—in other words, exposed to atmosphere). It is the number that counts in gas-phase extraction because the reaction is topochemical and can occur only on exposed surfaces of gold. The higher this measure of liberation, the larger the exposed surface available to the ligand for reaction. In Figure 3.3 the difference between liberation by free surface and liberation by grade is illustrated.

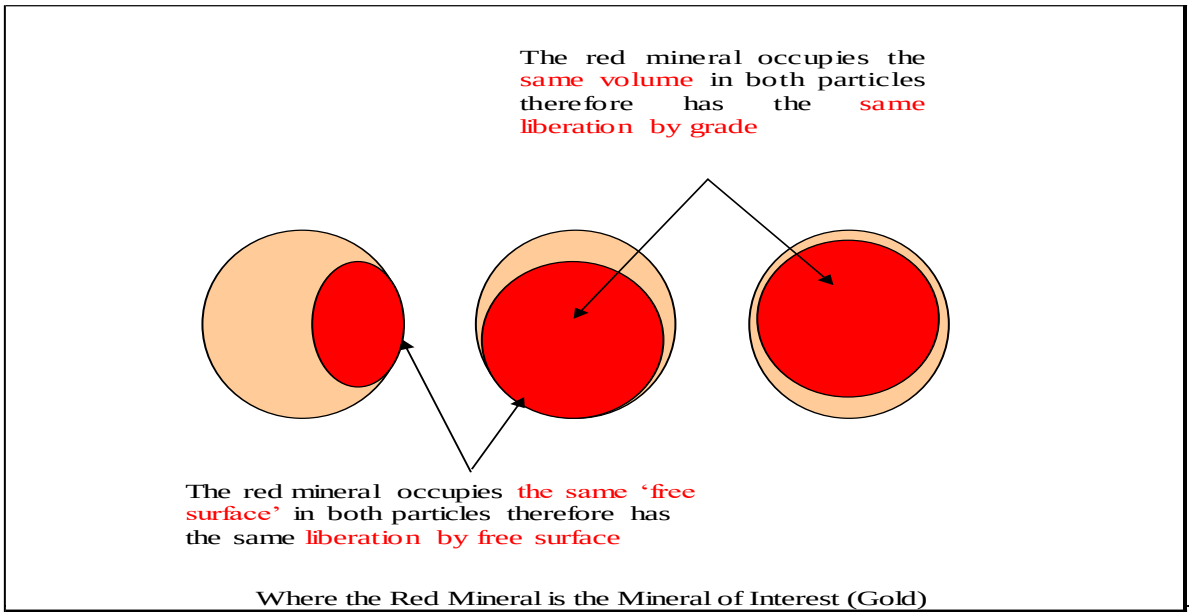

Figure 3. 3: Illustration of the difference between liberation by grade and liberation by a free surface

The liberation of gold by a free surface is highest for particles with size fractions <10 µm followed by particles in between 45 and 25 µm (see Figure 3.4).

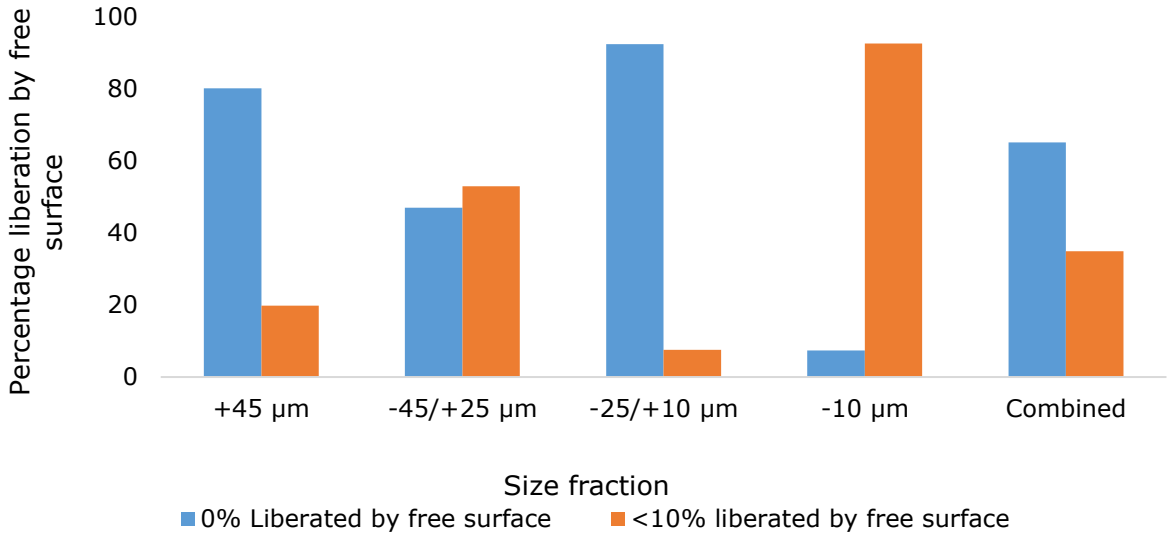

Figure 3. 4: DRDGold tailings, gold liberation by free surface

3.3 Experimental setup and procedure

Tests were done in a fixed bed reactor. The temperature in the fixed bed reactor was measured by thermocouples on the column. The temperature was kept between 190–250°C and was controlled by proportional integral differential (PID) controller. A carrier gas (compressed air) removed the volatile metal complexes resulting from the reaction. A condenser was incorporated into the set-up, solely to condense the vapor product. Gas-flow meters and a peristaltic pump were used to control the carrier gas flow and the flowrate of the ligand respectively.

The reactor was charged with (20 g, 10 g) of the tailing material. The reactor was preheated to temperatures between 150 and 280°C to vaporize the extractant. The ligand was then pumped into the reactor at a specific flow rate (3 mL/min). The temperatures were kept constant for a certain time for each extractant, to determine the kinetics of the reaction. After volatilization, the metal complex was collected in a cold trap. The trapped metal complex was analysed to determine the metal content. The reactor set up is shown in Figure 3.5.

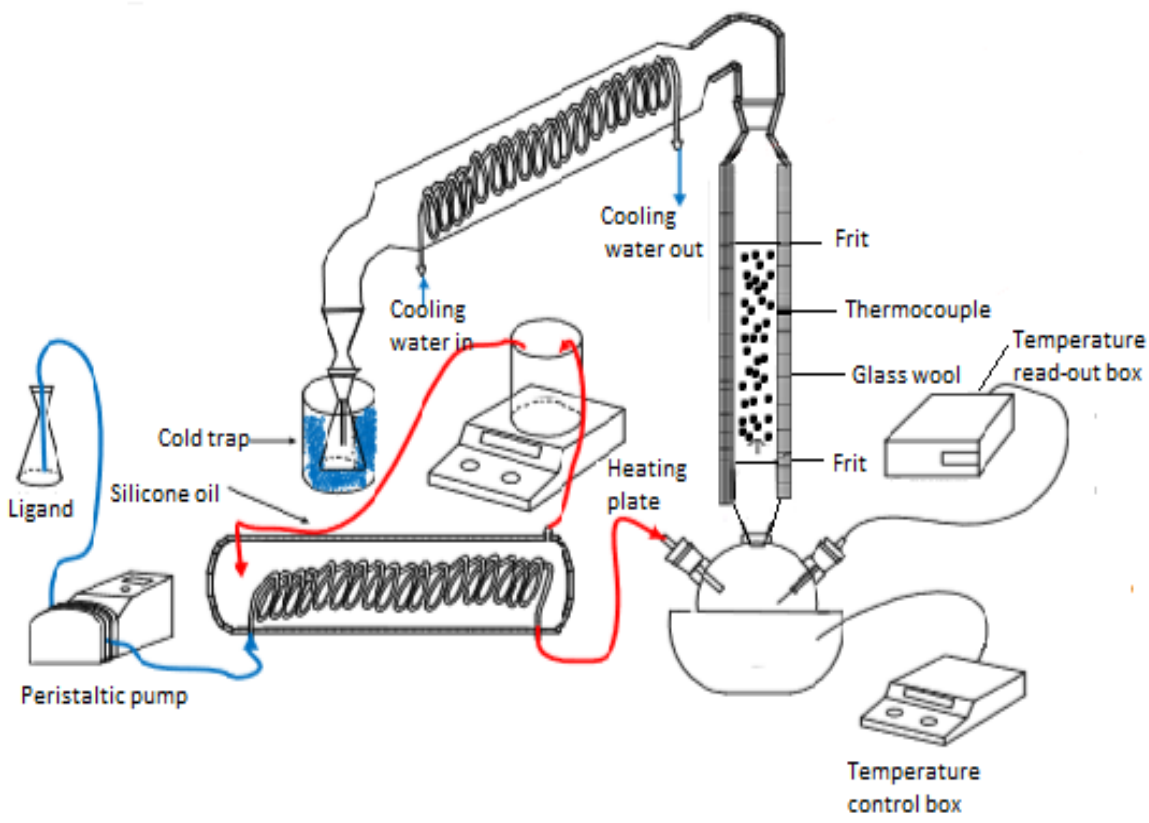

Figure 3. 5: Fixed bed reactor experimental set up (adapted from Olehile, 2017).

3.4 Analytical techniques for the detection of gold

Various analytical techniques can be used to detect metals and determine the content of metals in a sample. The method chosen for the detection of metals in this investigation is atomic absorption spectroscopy (AAS). The Initial gold content as determined by atomic absorption spectroscopy (AAS), is 0.30 g/t. This was done by digesting 1 g of the sample in 20 ml of aqua regia. The density was determined by helium pycnometer and was found to be 3.15 g/cm^3.

3.5 Liquid-phase extraction of gold

The liquid-phase extraction of gold from the tailings was carried out in a batch reactor (see Figure 3.6). The required volume of the acetylacetone to react with 20 g of the tailing material was determined and it was found to be 31 mL of acetylacetone.

The reagents—31 mL of acetylacetone (stoichiometric equivalent) and a 20 g of the tailing material—were placed in a 250 mL glass flask fitted with a reflux condenser. The flask was then heated using a heating plate, the temperature was varied from 80 to 140°C for different temperatures. The agitation speed was kept constant at 1083 rpm. The experimental run was carried on for 24 hours and after 24 hours the sample was analysed for the content of the gold with AAS.

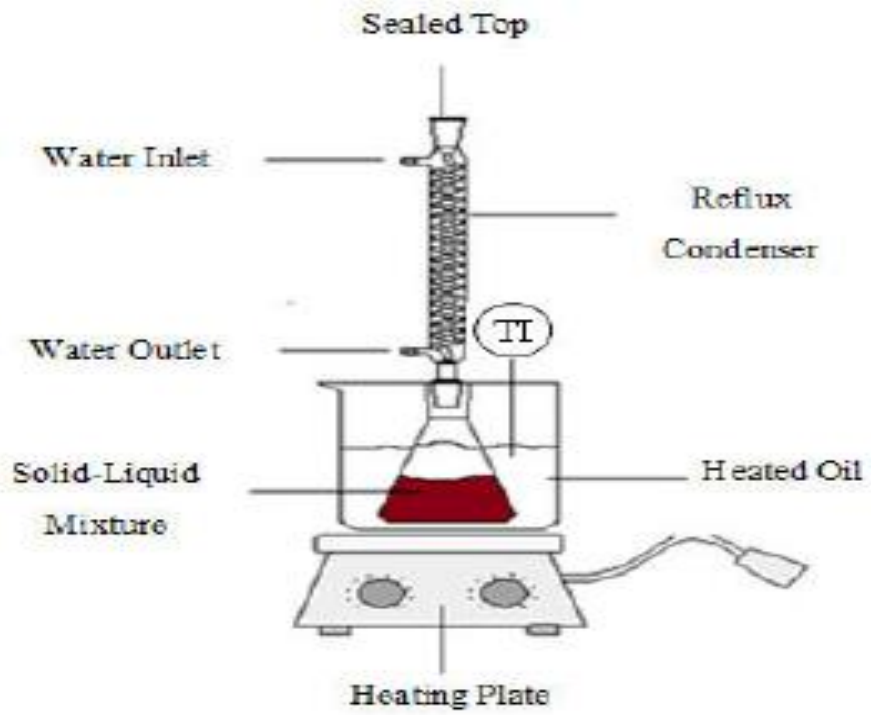

Figure 3. 6: Liquid phase extraction experimental set up (adapted from Tshofu , 2014).

4 RESULTS AND DISCUSSION

4.1 Gold(III)- β-diketonate complexes: A density functional theory study

In this section, for the first time to my knowledge, a DFT study on the structure and properties of three Au(III)- β-diketonato complexes, namely, Au(III) acetylacetonate, Au(III) trifluoroacetylacetonate, and Au(III) hexafluoroacetyl-acetonate is presented.

Geometry optimization

A density functional theory study on organometallic complexes can give insight if the complex may exist (energy) and the geometry of the complex, such as the arrangement of the ligands around the metal, as well as into the preferred spin state of the complexes. Selected Au β-diketonato complexes were optimized using the Gaussian 16 package (Frisch *et al.* 2009). The B3LYP (Becke, 1993; Stephens *et al.* 1994) functional and the Stuttgart/Dresden (SDD) (Fuentealba *et al.* 1982) basis set were used for all atoms. The DFT optimized geometry of Au(III)-(β-diketonato) complexes are presented in Figure 4.1, as (a) $Au(acac)_3$, (b) $[Au(acac)_2]^+$, (c) $Au(hfa)_3$, (d) $Au(tfa)_3$, where (acac=acetylacetone, hfa=hexafluoroacetylacetone, tfa=trifluoroacetylacetone).

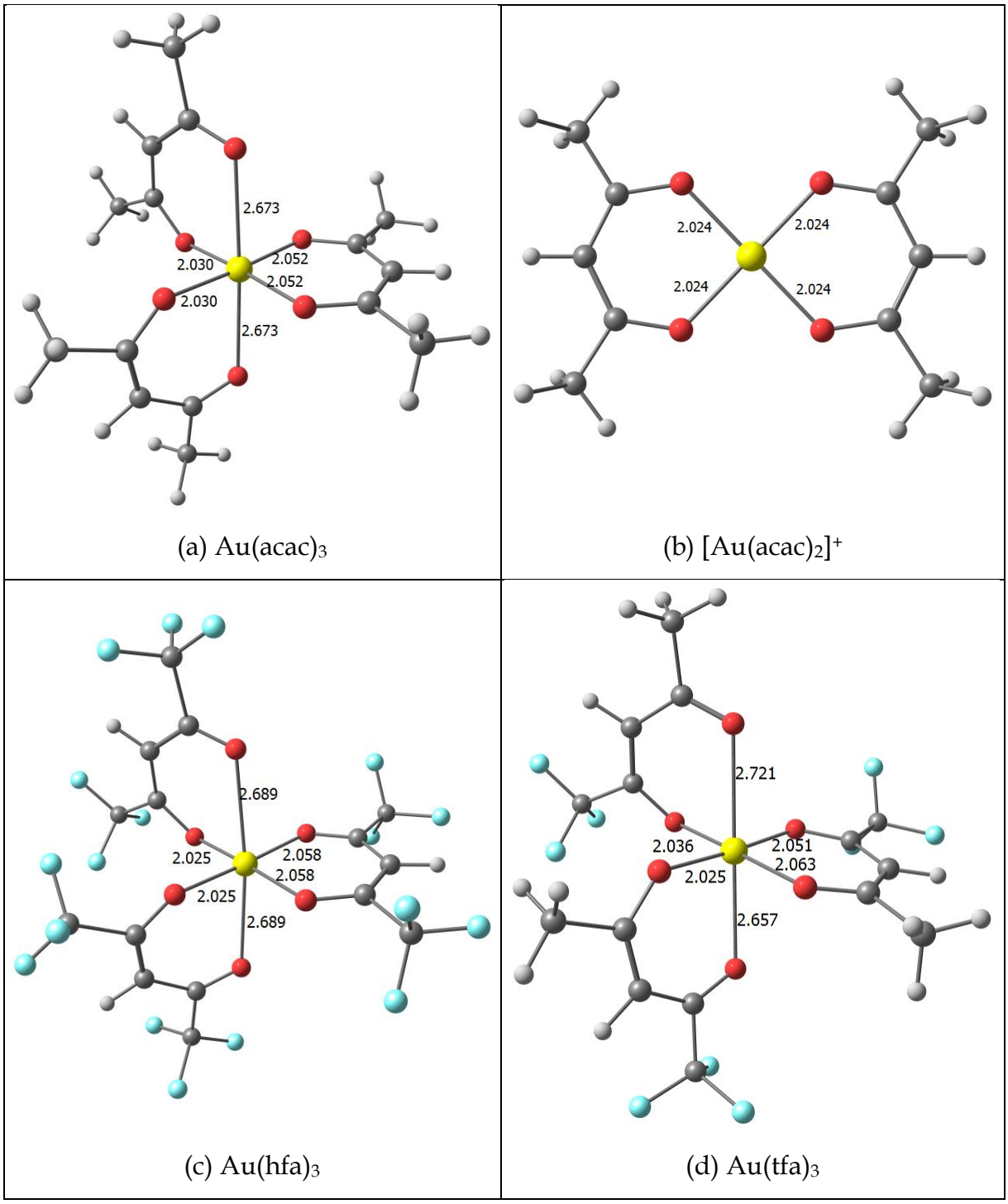

(a) $Au(acac)_3$ (b) $[Au(acac)_2]^+$

(c) $Au(hfa)_3$ (d) $Au(tfa)_3$

Figure 4. 1:B3lyp/SDD optimized geometry of the Au β-diketonato complexes. (a) $Au(acac)_3$, (b) $[Au(acac)_2]+$, (c) $Au(hfa)_3$, (d) $Au(tfa)_3$, showing selected bond lengths in Å. Colour scheme used for atoms: Au (yellow), C (grey), H (white). (acac=acetylacetone, hfa=hexafluoroacetylacetone, tfa=trifluoroacetylacetone)

Table 4.1 tabulates the DFT-calculated bond lengths and angles of Au(III)$(acac)_2^+$ and Au(III)$(acac)_3$. The O-Au-O bond angles for $Au(acac)_2^+$ are 92.8°, which is close to the bond angles expected for square planar complexes (90°). All of the Au-O bond lengths for the $Au(acac)_2^+$ are found to be the same as reported in Table 4.1. Therefore, the $Au(acac)_2^+$ can said to be a square planar complex (see Figure 4.2). The average O-Au-O bond angles for $Au(acac)_3$ was found to be 86.51°. This compares favourably—the deviation is slight—to the bond angles expected for an octahedral complex (90°).

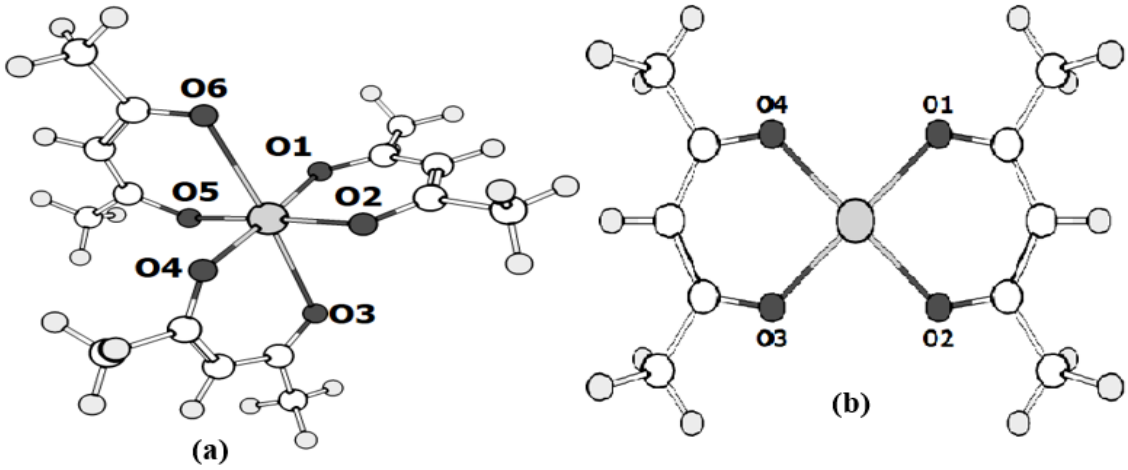

Figure 4. 2: Perspective drawing of the molecular structures of a) $Au(acac)_3$ and b) $[Au(acac)_2]+$ showing selected atom numbering.

Table 4. 1: Selected DFT bond lengths and angles for $[Au(acac)_2]+$ and $Au(acac)_3$. Atom numbering is shown in Figure 4.2.

Bond	$[Au(acac)_2]^+$	$Au(acac)_3$
Bond length (Å)		
Au-O(1)	2.024	2.052
Au-O(2)	2.024	2.052
Au-O(3)	2.024	2.673
Au-O(4)	2.024	2.030
Au-O(5)		2.030
Au-O(6)		2.673
Bond angle (°)		
O(1)-Au-O(2)	92.80	92.66
O(3)-Au-O(4)	92.80	83.44
O(5)-Au-O(6)		83.44
Average bond angles		86.51

Molecular orbital

Molecular orbital theory (MO) is a theory that can be applied to explain the bonding of complex molecules. In MO theory the molecular orbitals are made from linear combination of atomic orbitals (Shriver *et al.* 2010). It describes an area around two or more atoms where the probability of finding an electron is high. Highest occupied molecular orbital (HOMO) is an orbital which acts as donor site where electrophiles can attack and lowest unoccupied molecular orbital (LUMO) is an orbital which acts as an acceptor where nucleophiles can attack (Fukui *et al.* 1952). The DFT calculated HOMO and LUMO of $[Au(acac)_2]^+$, $Au(acac)_3$, $Au(tfa)_3$, $Au(hfa)_3$ are presented in Figures 4.3-4.6. The LUMO of all four complexes is of $d_{x^2-y^2}$ character. The HOMO of $Au(acac)_3$, HOMO of $Au(tfa)_3$ and the HOMO-1 of $Au(hfa)_3$ are of d_{z^2} character. The top three HOMOs of $[Au(acac)_2]^+$ is ligand based, while the HOMO-3 is of d_{z^2} character.

The difference in energy between the HOMO and LUMO is called the HOMO-LUMO gap and is an indication of the strength of the transition metal complex. A large HOMO−LUMO gap implies high kinetic stability and low chemical reactivity of the complex, because it is energetically unfavourable to add electrons to a high-lying LUMO, to extract electrons from a low-lying HOMO, in order to form the activated complex of any potential reaction (Aihara, 1999). The HOMO-LUMO gaps of the studied complexes have been calculated (see Table 2). The HOMO-LUMO gap of the Au(III)(β-diketonato)$_3$ complexes is very similar, showing similar stability of the three complexes. Conradie and Conradie (2015) found that for Fe(β-diketonato)$_3$ complexes the more acidic the ligand attached to the metal is the more electron density is withdrawn from the metal center and the lower the LUMO energy of the complex. The Au (β-diketonato)$_3$ complexes of this study showed the same trend (see table 4.2).

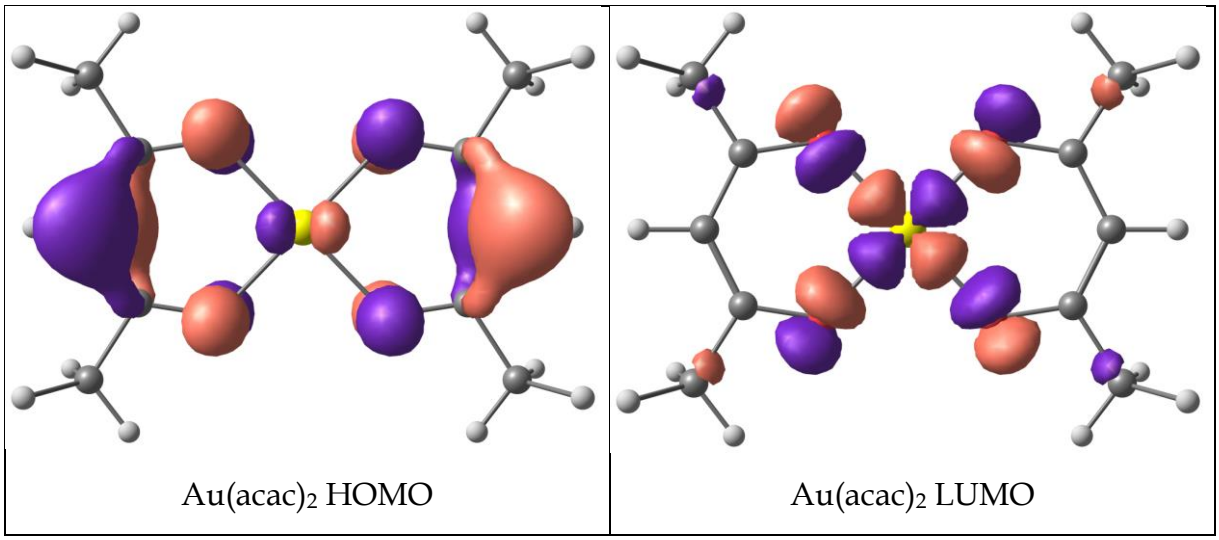

Au(acac)$_2$ HOMO | Au(acac)$_2$ LUMO

Figure 4. 3: The DFT drawn HOMO and LUMO of Au(acac)$_2$. Colour scheme used for atoms: Au (yellow), C (grey), H (white). A contour of 0.05 eÅ-3 was used for the MO plots.

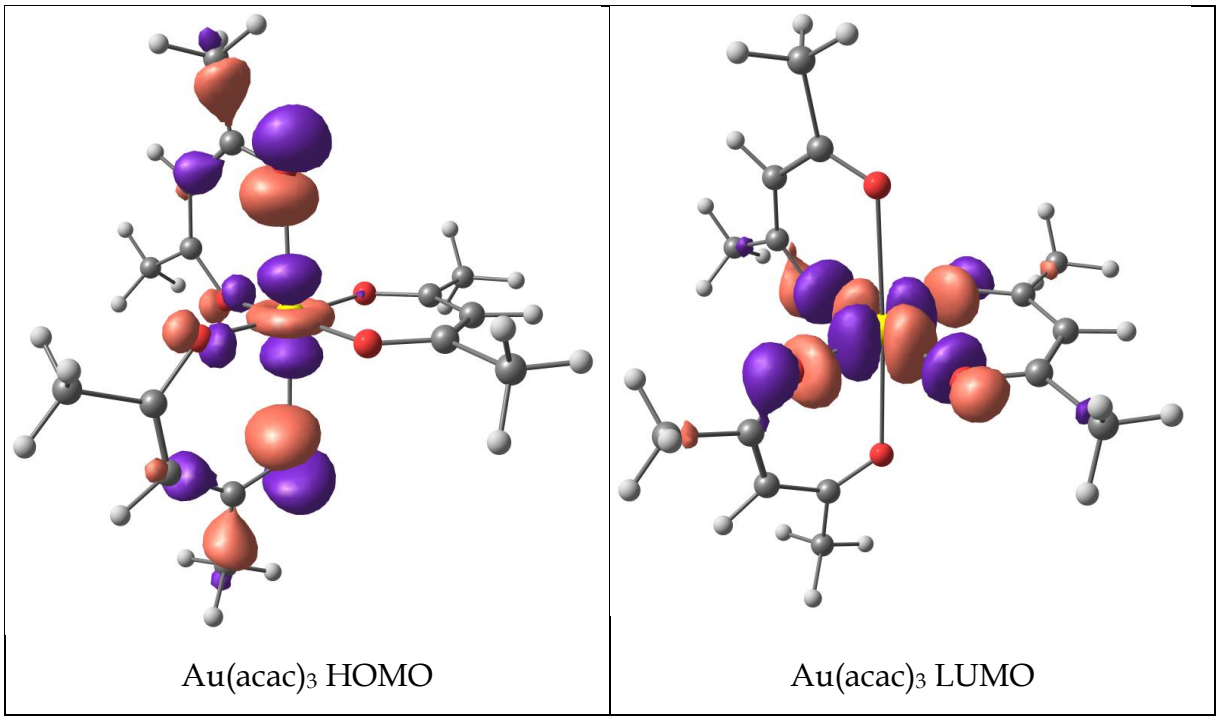

Au(acac)$_3$ HOMO | Au(acac)$_3$ LUMO

Figure 4. 4: The DFT drawn HOMO and LUMO of Au(acac)$_3$. Colour scheme used for atoms: Au (yellow), C (grey), H (white). A contour of 0.05 eÅ-3 was used for the MO plots.

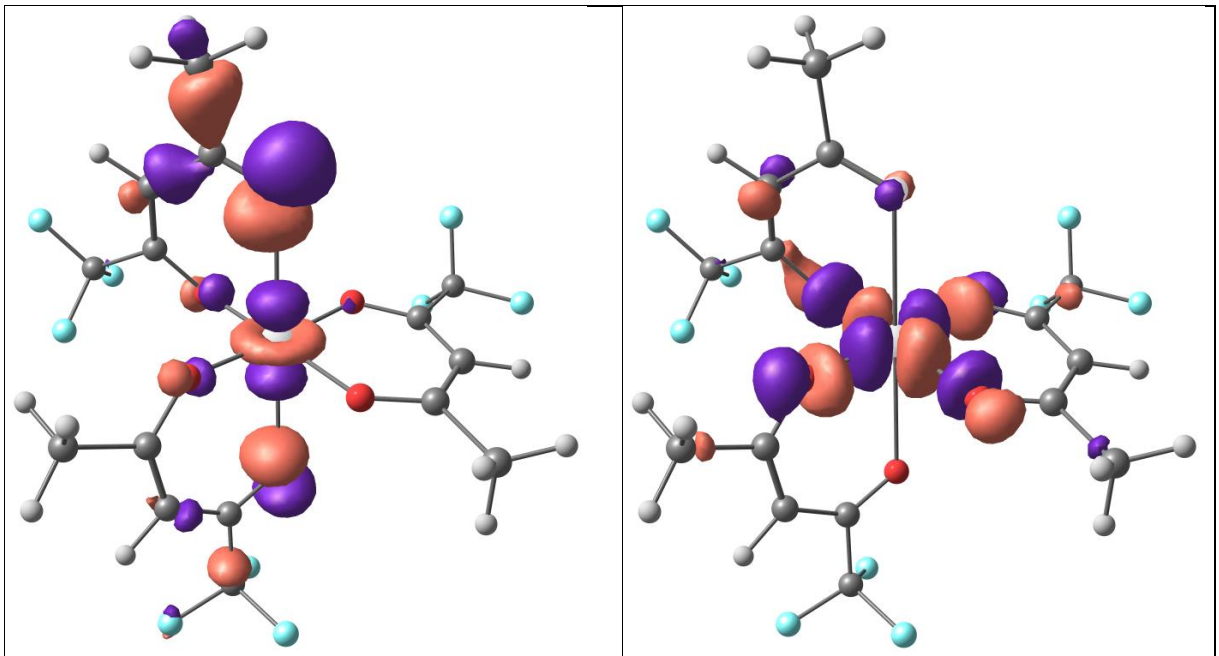

Figure 4. 5: The DFT drawn HOMO and LUMO of $Au(tfa)_3$. Colour scheme used for atoms: Au (yellow), F (blue), C (grey), H (white). A contour of 0.05 eÅ-3 was used for the MO plots.

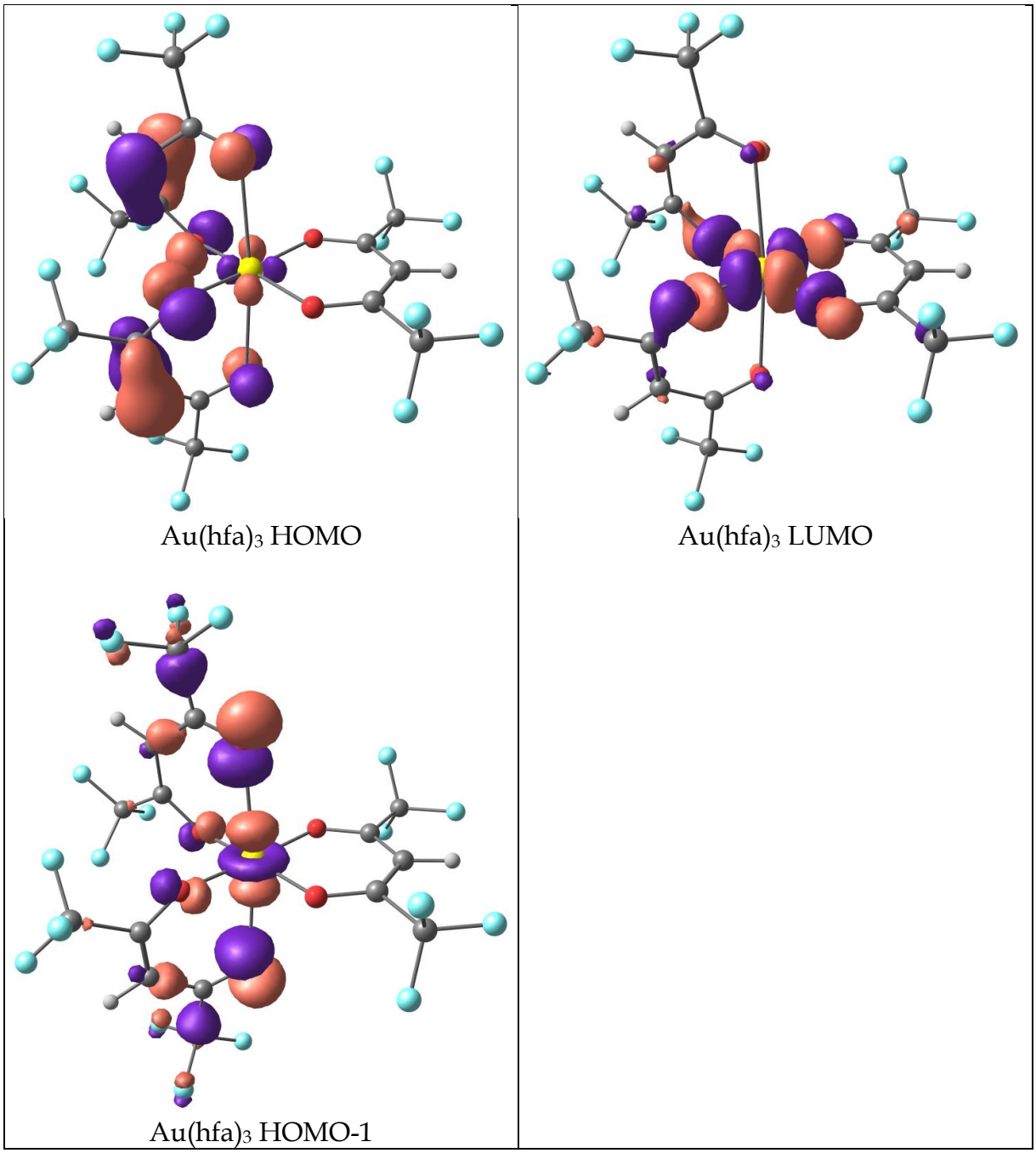

Figure 4. 6: The DFT drawn HOMO, HOMO-1 and LUMO of $Au(hfa)_3$. Colour scheme used for atoms: Au (yellow), F (blue), C (grey), H (white). A contour of 0.05 eÅ-3 was used for the MO plots

Table 4. 2: DFT calculated HOMO, LUMO and HOMO-LUMO gap energies (eV) of the Au(β-diketonato)$_3$ complexes studied

β-diketonate complex	HOMO energy (eV)	LUMO energy (eV)	HOMO–LUMO gap (eV)
Au(acac)$_3$	−5.79	−3.18	2.61
Au(tfa)$_3$	−7.27	−4.62	2.61
Au(hfa)$_3$	−8.66	−6.05	2.65

Enthalpy and Gibbs free energy

The reaction electronic energy (*E*), Gibbs free energy (*G*) and enthalpy (*H*) of two proposed reactions between Au^{3+} and deprotonated aceytylacetone (see reactions 4.3 and 4.4) were calculated from DFT calculated energies. Reactions 4.3 and 4.4 are both spontaneous and exothermic. However, reaction 4.3 is slightly more likely to occur, in other words, $[Au(C_5H_7O_2)_3]$ is easier to form than $[Au(C_5H_7O_2)_2]^{+1}$. It must be noted that these reactions assume that Au(III) ions and the acac anion are available in the reaction mixture and that there are no other ions or ligands in the reaction mixture that could influence the reaction.

$$Au^{3+} + 3(C_5H_7O_2)^- \rightarrow [Au(C_5H_7O_2)_3] \quad [4.3]$$

$$\Delta H_{rxn1} = -60.4\ eV,\ \ \Delta G_{rxn1} = -58.9\ eV,\ \Delta E_{rxn1} = -60.7\ eV,$$

$$Au^{3+} + 2(C_5H_7O_2)^- \rightarrow [Au(C_5H_7O_2)_2]^{+1} \quad [4.4]$$

$$\Delta H_{rxn2} = -56.0\ eV,\ \ \Delta G_{rxn2} = -54.7\ eV,\ \ \Delta E_{rxn2} = -56.1\ eV,$$

DFT calculations also showed that both Au(acac)$_2^+$ and Au(acac)$_3$ complexes are diamagnetic as the energy of the optimized singlet is lower than the energy of the optimized triplet (energy values are listed in Table 4.3).

Table 4. 3: DFT calculated energy (eV) and Gibbs free energy (eV) values of the different spin states of the Au β-diketonate complexes studied

β-diketonate complex	Energy E (eV)		ΔE	Gibbs free energy G (eV)		ΔG
spin (multiplicity)	0 (1)	1 (3)		0 (1)	1 (3)	
$[Au(acac)_2]^-$	−22466.24	−22465.12	1.13	−22467.80	−22466.82	0.98
$Au(acac)_3$	−31860.34	−31860.25	0.10	−31862.87	−31862.73	0.13
$Au(tfa)_3$	−56166.74	−56166.62	0.12	−56169.75	−56169.64	0.11
$Au(hfa)_3$	−80472.33	−80472.16	0.17	−80475.72	−80475.63	0.08

Summary

DFT calculations showed that both $[Au(acac)_2]^-$ and $Au(acac)_3$ can exist under the correct reaction conditions. However, $Au(acac)_3$ complex is energetically favoured. The $[Au(acac)_2]^-$ complex is square planar, the $Au(acac)_3$ is octahedral. Furthermore, the HOMO-LUMO gap of the Au(III)(β-diketonato)$_3$ complexes have been calculated and are similar, showing similar stabilities for the three complexes.

4.2 Preliminary fluidization tests

The gold content of the tailings, determined by atomic absorption spectroscopy (AAS), is 0.30 g/t. The density was determined by helium pycnometer and was found to be 3.15 g/cm^3. The gold is either native or alloyed with silver in electrum. Some of it is 'liberated'—a significant fraction of its surface is exposed; other particles of gold are locked, usually in pyrite (FeS_2). The gold in liberated particles, because they are exposed to a gas or liquid phase, can react with a ligand and so be extracted. Tests were conducted to assess the behaviour of beds of tailings—the particles of which are very fine—under the action of an upwardly flowing gas (air). Particle density and size place the material (tailings) in group C of Geldart's classification (see Figure 4.7, Geldart 1973). Beds of these particles do not fluidize or are difficult to fluidize. The reason for the aversion is the strongly acting forces of cohesion, forces that are Van der Waals and electrostatic in nature. With fine particles these forces are orders of magnitude greater than drag and gravitational forces arising from an upwardly

flowing gas acting on solids. Strongly cohesive forces promote channelling and agglomerates in the bed.

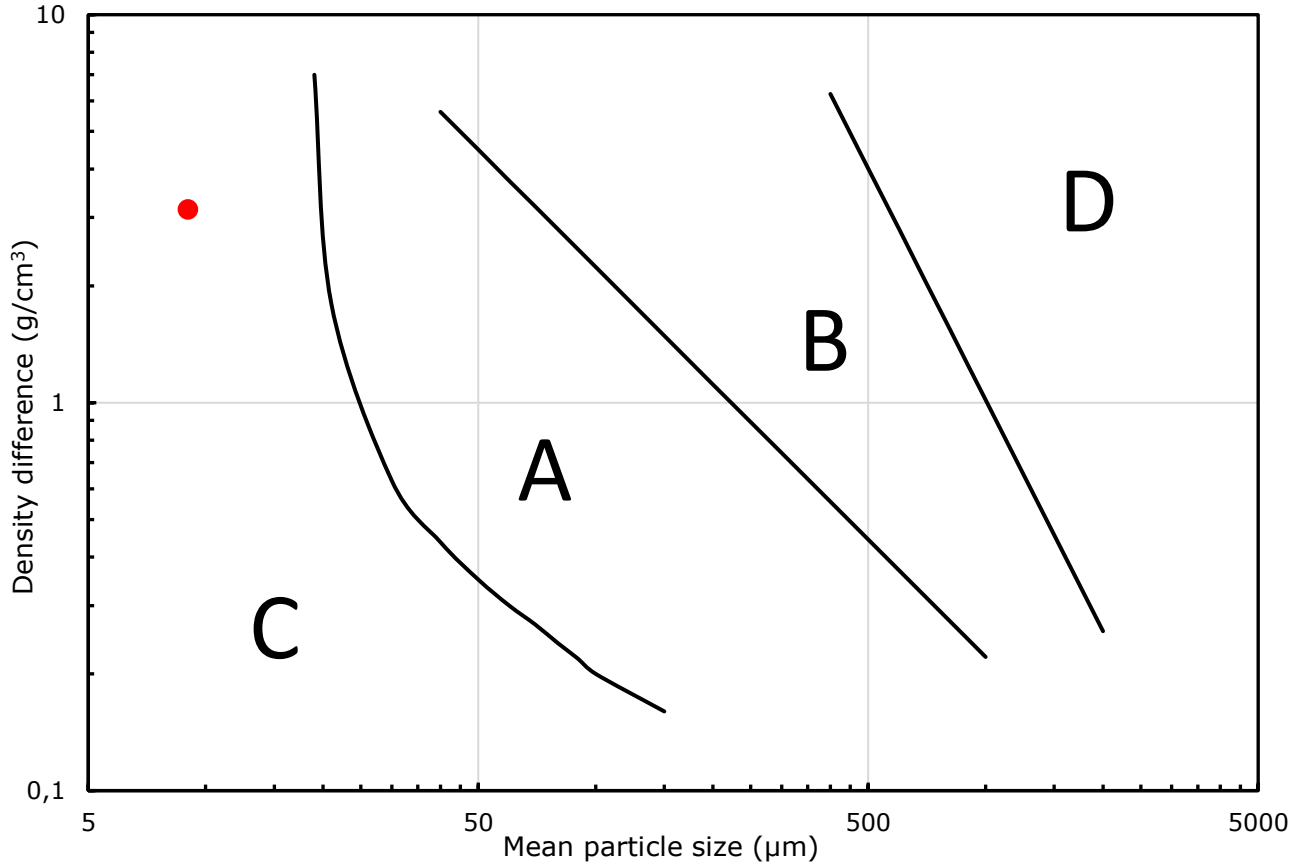

Figure 4. 7: Geldart classification chart (Geldart 1973). The red dot denotes the tailing material

The particle size distribution of the tailing was obtained by laser diffraction. Particle sizes ranged from less than 1 µm to over 300 µm (see Figure 4.1). The defining indices are d_{20}, d_{50} and d_{80} of 3 µm, 16 µm and 91 µm, respectively.

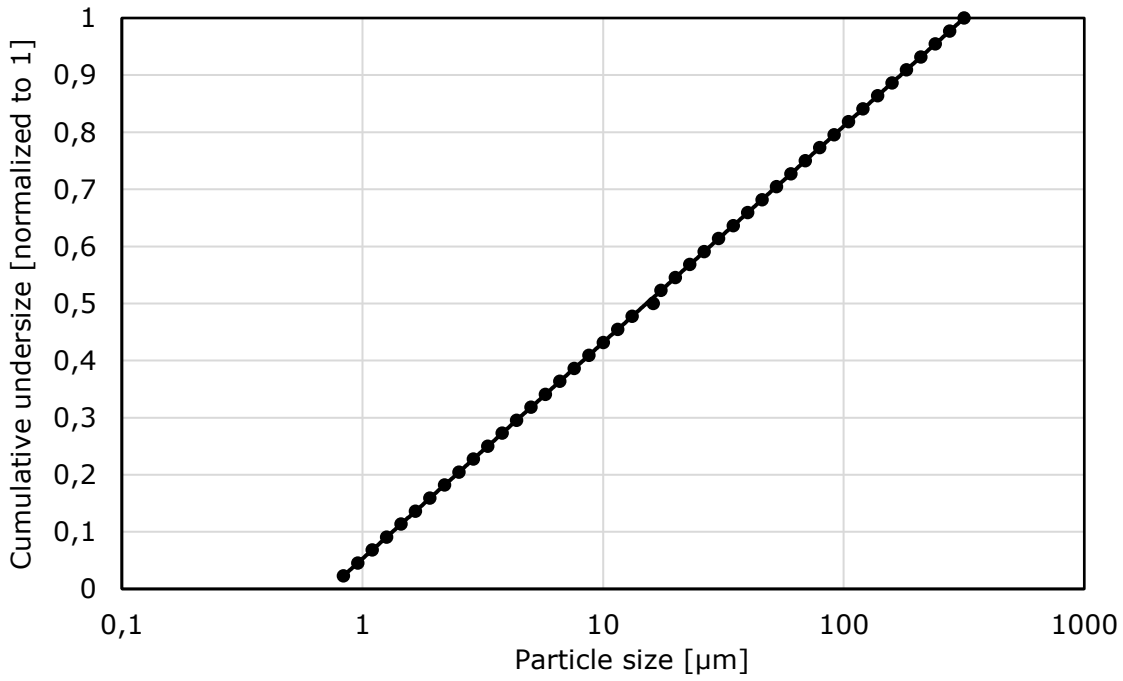

Figure 4. 8: Distribution curve of the particle size of the tailings (by laser diffraction)

First, the tailings sample as is was placed on the distributor. The bed did not fluidize, and channels formed. This is because the material falls into group C of Geldart classification. These fine particles are cohesive and the Van der Waals forces are much greater than drag and gravitational forces acting on the particles. The strong inter-particle forces led to channelling and the formation of agglomerates in the bed. To improve fluidization of the tailings, coarser particles (inert material), namely sand (53 µm and 106 µm), was introduced into the bed and a binary mixture of the tailings and the sand was obtained.

The binary mixtures of sand (53 µm, 106 µm) and the tailings were tested. The mass of fine material carried from the bed was measured over intervals of time for 10 minutes. Material left the bed from the moment a test started (see Figure 4.2). The rate is slightly higher for the coarser bed stabilizer—2.7 g/min compared with 2.4 g/min.

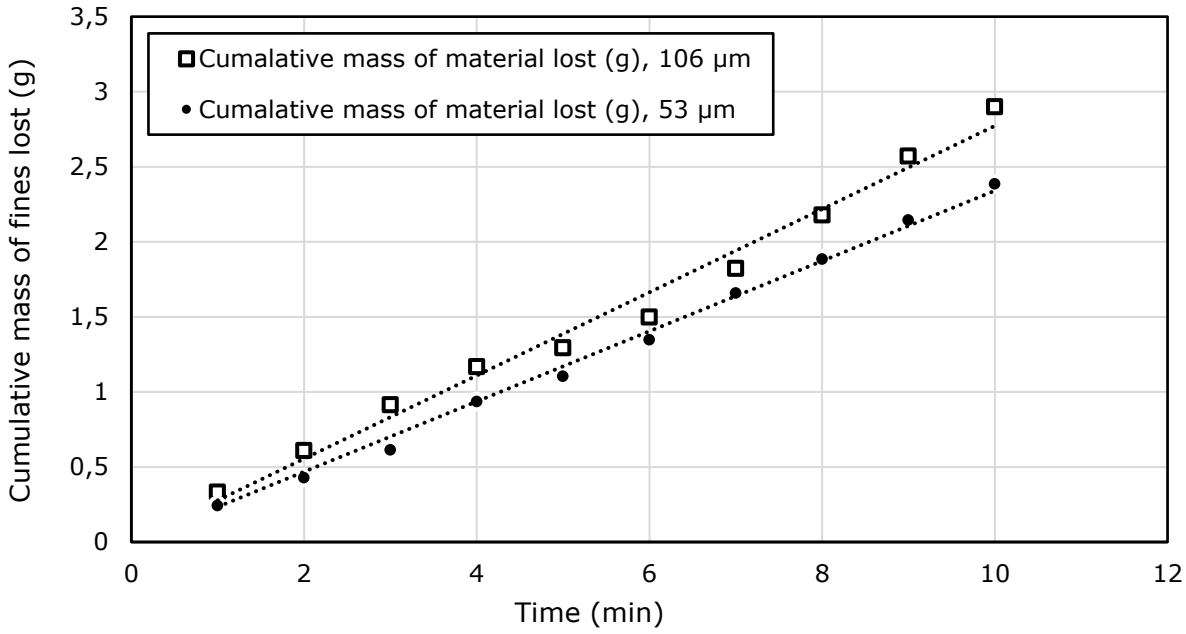

Figure 4. 9: Cumulative mass of material lost for the 106 µm and 53 µm sand with the tailings in the first 10 minutes

For the 106 µm sand bed more material is lost than with the 53 µm sand. This is because the gas is at a higher velocity for the 106 µm (0.02 m/s) than the 53 µm (0.015 m/s) and therefore there are more bubbles present in the bed. However, there is still a loss of material for the 53 µm sand, since there are bubbles still present in the bed. For both size fractions, the particles did not stay long in the bed and were carried out by bubbles. Bubble size is important in understanding fluidization as it directly affects reactor performance. Bubbling also decreases the mass transfer in the fluidized bed (Van Ommen *et al.* 2012).

Getting rid of these bubbles to obtain smooth fluidization was difficult in apparatus at bench scale. A fixed bed reactor designed to hold about 20 g of the tailings material was fabricated. Further tests were carried out in this reactor.

4.3 Gold extraction results

The extraction of gold from tailings using volatile β-diketone ligands was carried out in both liquid and gas phases. These ligands were chosen because studies have shown that β-diketone ligands such as acetylacetone and its derivatives could be used as the volatile ligand in the process. Furthermore, the DFT study (section 4.1) showed that the three different β-diketones investigated have similar stabilities; therefore, only acetylacetone was used as the gas-phase extractant as it is the cheapest of the three ligands tested. The gas-phase and liquid-phase experiments were carried out as outlined in chapter 3. In the gas phase, the acetylacetone ligand was introduced into the fixed bed as a vapour. The reaction between acetylacetone and gold is thought to be as follows:

$$2Au + 3O_2 + 6H(C_5H_8O_2) \rightarrow 2Au(C_5H_7O_2)_3(s) + 6H_2O\ (g)\ldots\ldots\ldots\ldots \quad [4.5]$$

The effects of temperature, bed mass, and the type of β-diketone on the rate of extraction were measured.

4.3.1 Liquid-phase extraction

Effect of temperature

As expected, the extent of extraction increases with temperature—to a maximum of 140°C, the boiling point of acetylacetone (see Figure 4.10. The increase in extraction, however, is not that large. It rises only 5% from 80 to 140°C for acetylacetone. Tshofu (2014), who tested the liquid-phase extraction of iron from iron ore fines with acetylacetone, found that the highest extraction was obtained at this highest temperature, 140°C. The results observed for this work can be explained by the fact that only the gold with at most 10% of its surface exposed to the ligand is extracted in liquid-phase extraction. Of that, only 35% of the gold is liberated for the combined size fraction as shown in figure 3.5. In the liquid-phase extraction, we are getting extractions of up to 25% that is about 70% of the liberated gold over 24 hours.

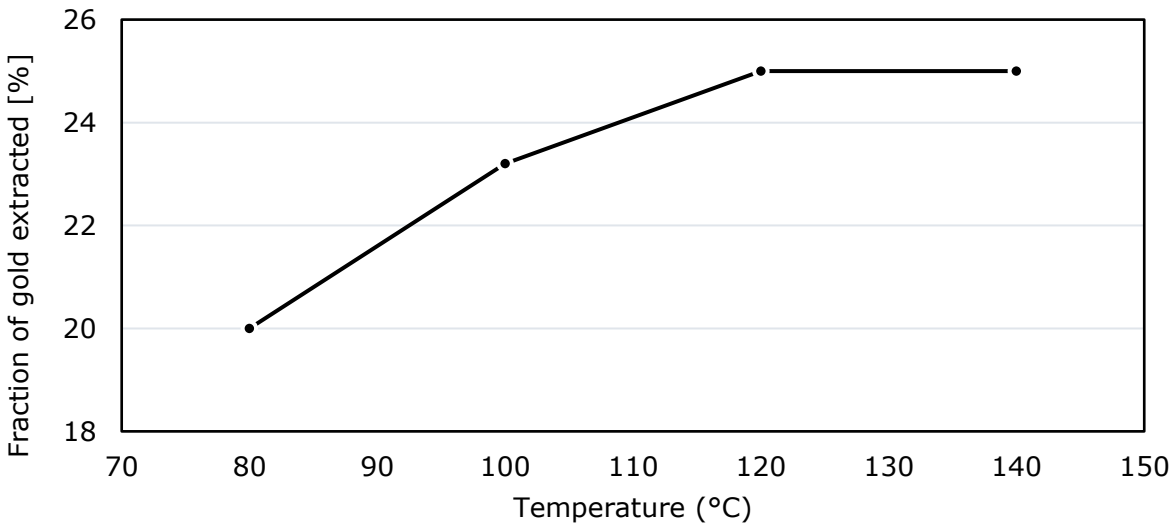

Figure 4. 10: Liquid-phase extraction of gold with acetylacetone as a function of temperature

Effect of β-diketone type

Extraction tests in the liquid phase were carried out with three β-diketone ligands—hexafluoroacetylacetone (HFA), trifluoroacetylacetone (TFA), and acetylacetone (ACAC). The tests were run with 2 g of sample (tailings) and a solid-to-liquid ratio of 1/4. The experiment was conducted at the respective boiling points of the three β-diketonato ligands. HFA gave the highest extraction (18%) after 24 hours (see Figure 4.11). At 17% TFA is a close second.

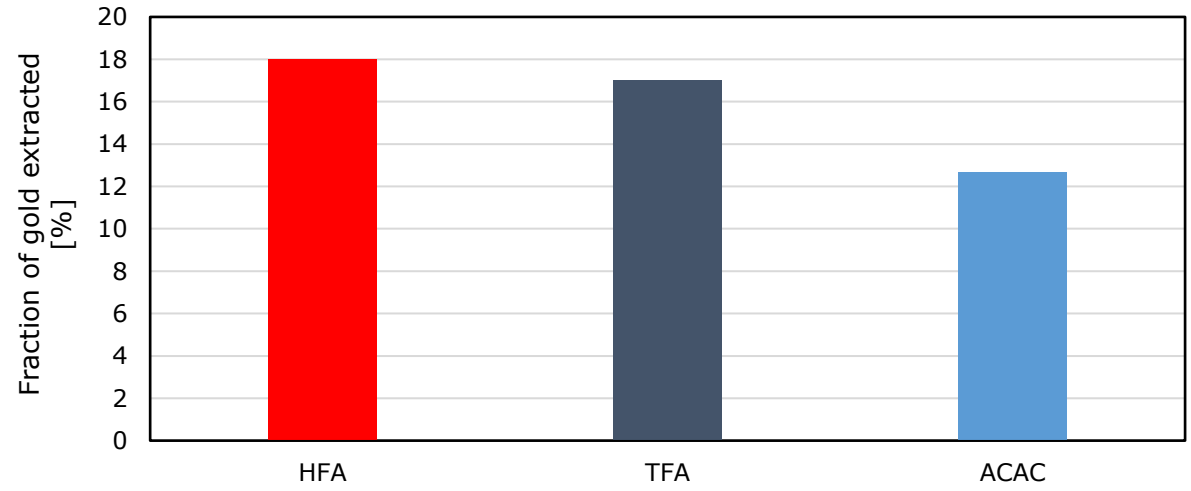

Figure 4. 11:Effect of β-diketone ligand type on the liquid-phase extraction of gold

The slightly higher extraction of the HFA and TFA can be explained by the fact that fluorinated β-diketonate complexes have greater volatility and thermal stability than the non-fluorinated β-diketonates. The highly electronegative perfluoromethyl groups in TFA and HFA lead to the tautomerization of these β-diketonates (Wallen *et al.* 1997). HFA is a fluorinated, bidentate β-diketonate ligand and, as discussed in Chapter 2, can be found as a ketone and an enol tautomer. For β-diketones, the enol-tautomer is usually favoured; however, for HFA the trifluoromethyl group causes an increase in the enol tautomer, so much so that some researchers have even predicted that HFA exists entirely in the enol tautomer (Ivankovits, 2000). The highly electron withrawing (fluorine) group on hexafluoroacetylacetone lead to increased Lewis acidity on the metal center. The extraction of metals with these β-diketone ligands is expected to increase in the order of acac < tfa < hfa. This agrees with the results found by other researchers (Wallen *et al.* 1997).

4.3.2 Gas-phase extraction

Effect of temperature

The extraction of gold was measured at temperatures of 190, 210, and 250°C (see Figure 4.12). The flow rate of ligand was held at 3 mL/min; the mass of the bed was held at 20 g. The rate of extraction increases with temperature to about 3 hours. There is little or no further extraction for longer times.

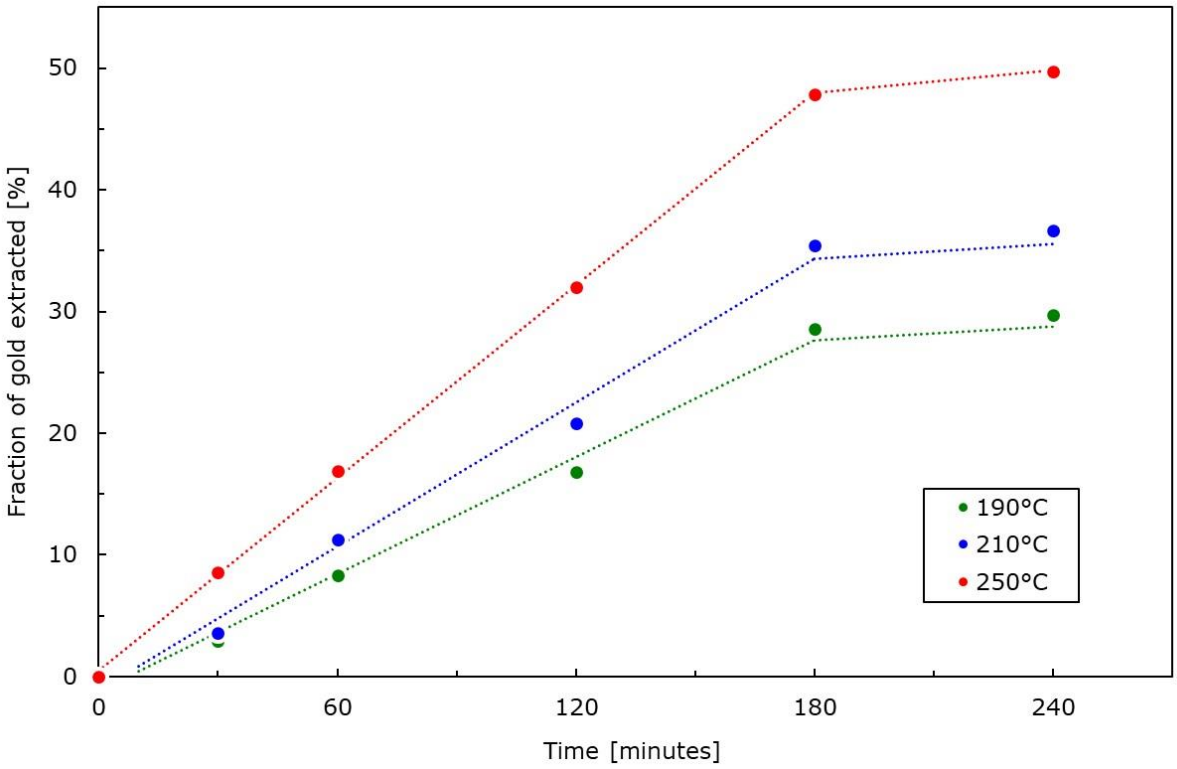

Figure 4. 12: The effect of temperature on the extraction of gold with (3 mL/min, 20g)

Van Dyk *et al.* (2012), extracting iron from iron ore fines, and Shemi *et al.* (2012), extracting aluminium from fly ash, in a gas phase with acetylacetone, observed similar trends.

The low recovery of gold in the tailing material is due to the poor liberation of gold, the presence of a significant amounts of quartz, which is a reagent consumer, and the fact that more than a third of the gold is locked in the sulfidic mineral pyrite (FeS_2). Leaching gold from refractory ore is generally difficult. The ERGO plant has an LGS (low-grade stream) and an HGS (high-grade stream). In the LGS only about 25% of the gold is recovered. This is because the gold is associated with different minerals and this means that the gold is encapsulated in other minerals like pyrite and quartz and therefore not available for the ligand (Mawire, 2019). Pyrite is the most common mineral in which gold is encapsulated. Figure 4.13 shows gold locked in pyrite.

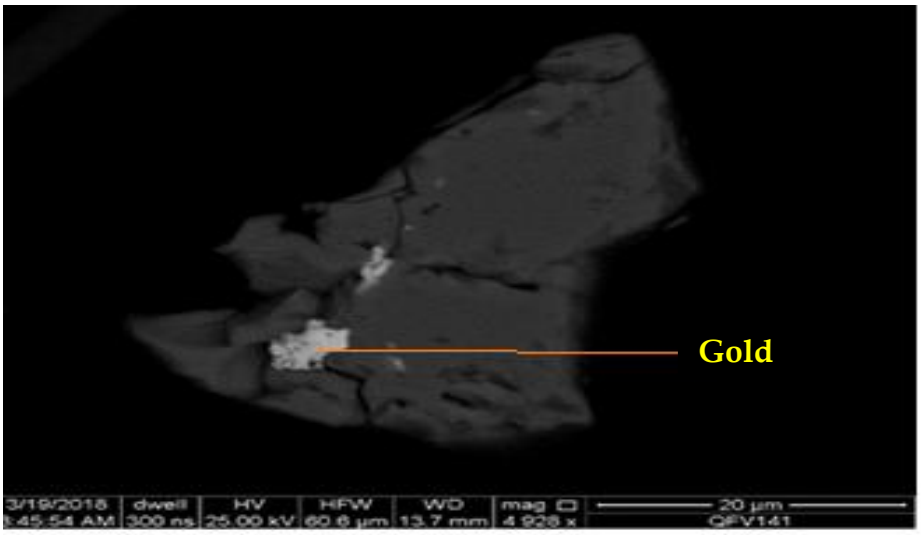

Figure 4. 13: Backscattered-electron image of gold

Effect of bed mass

When the bed mass was halved (from 20 g to 10 g) the rate of extraction increased slightly (see Figure 4.14; the tests were run at 210°C with the ligand flow rate held at 3 mL/min).

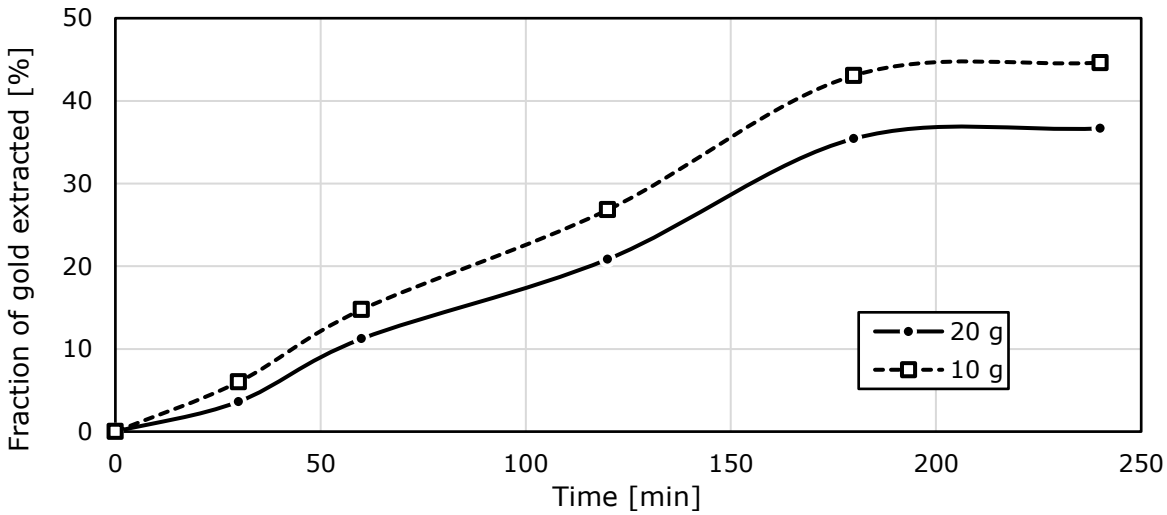

Figure 4. 14: The effect of bed mass on the extraction of gold with acetetylacetone ligand (3 mL/min, 210°C)

This is to be expected, as more of the ligand is available to react with the 10 g bed weight as compared to the 20 g bed weight, therefore the probability of a gold particle colliding with a molecule of the acetylacetone is higher for the smaller bed weight.

Solid analysis

SEM images of the residues were obtained to determine whether the ligand had been adsorbed on the surface of the particle and broke down the pyrite particles. Figure 4.15 and Figure 4.16 show secondary-electron images and an X-ray diffractogram of the tailings before and after the gas-phase extraction with acetylacetone respectively. Before gas-phase extraction the surface is smooth and has more structure with fewer pores and defects and one can clearly see the presence of pyrites; however, after gas-phase extraction there is a decrease in pyrite particles, and erosion of surface pores and pits can also be observed on the pyrite particles. Additionally, the results from SEM-EDS showed that the amount of sulfur was higher after the gas-phase extraction than before the extraction (see Figure 4.15). The iron content decreased after the gas-phase extraction, this is an indication that the ligand breaks down pyrite. The advantage, that refractory gold can be extracted by *acac*, is offset by a penalty, that some of the ligand is consumed by iron, as can be seen by the decreased ratio of Fe:S before and after extraction on the energy dispersive X-ray spectroscopy (EDS), Figure 4.15.

The major minerals are quartz and pyrite (see Figure 4.16). From the X-ray diffractogram in Figure 4.16 we can see that there is a decrease in the intensity of the pyrite peaks after the gas-phase extraction. The evidence is consistent with a breaking down of pyrite. There is also an indication that quartz might be attacked since the peaks for quartz also decreased.

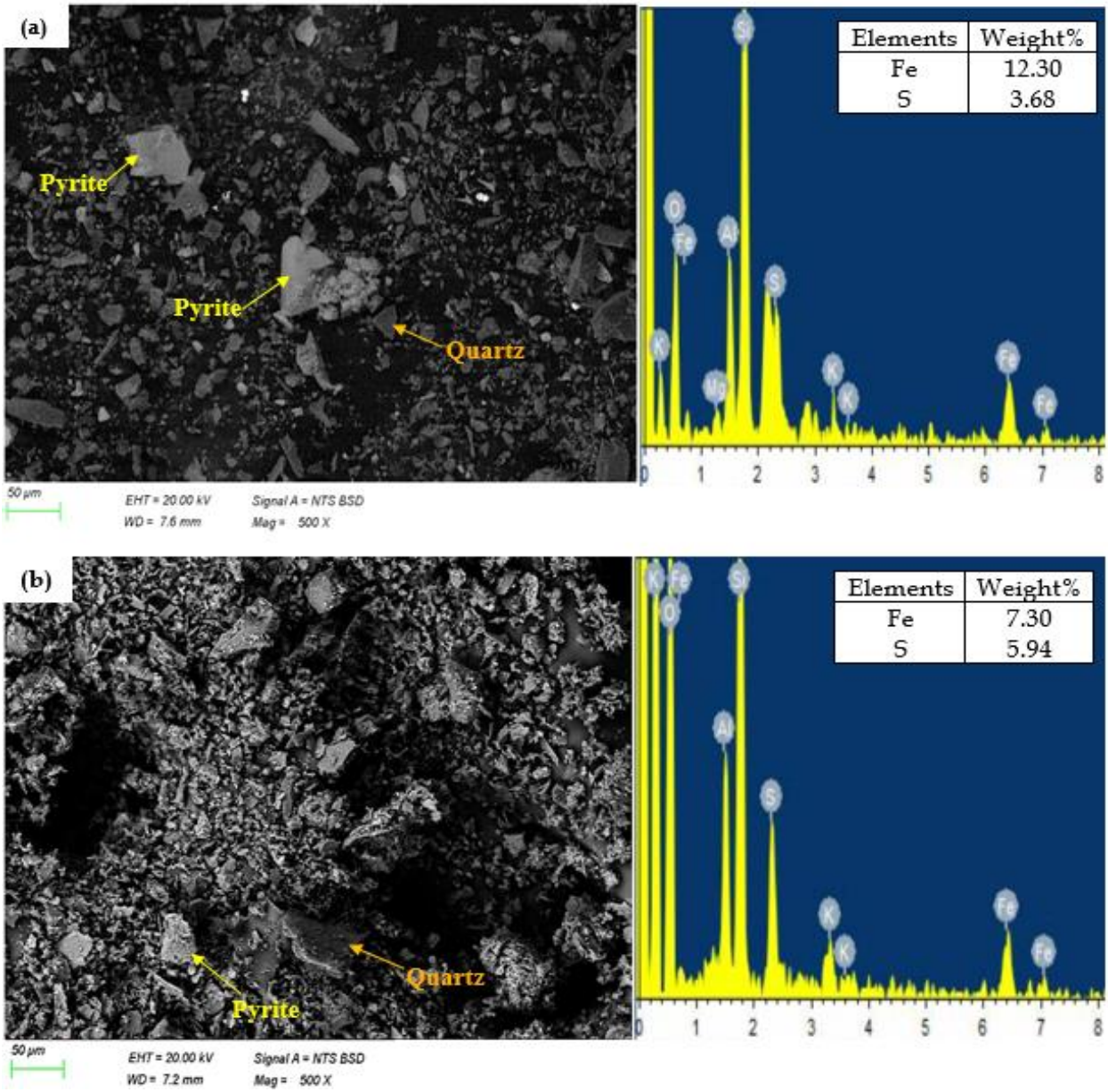

Figure 4. 15: Secondary-electron images of the tailings and EDS (a) before gas-phase extraction and (b) after gas-phase extraction with acetylacetone

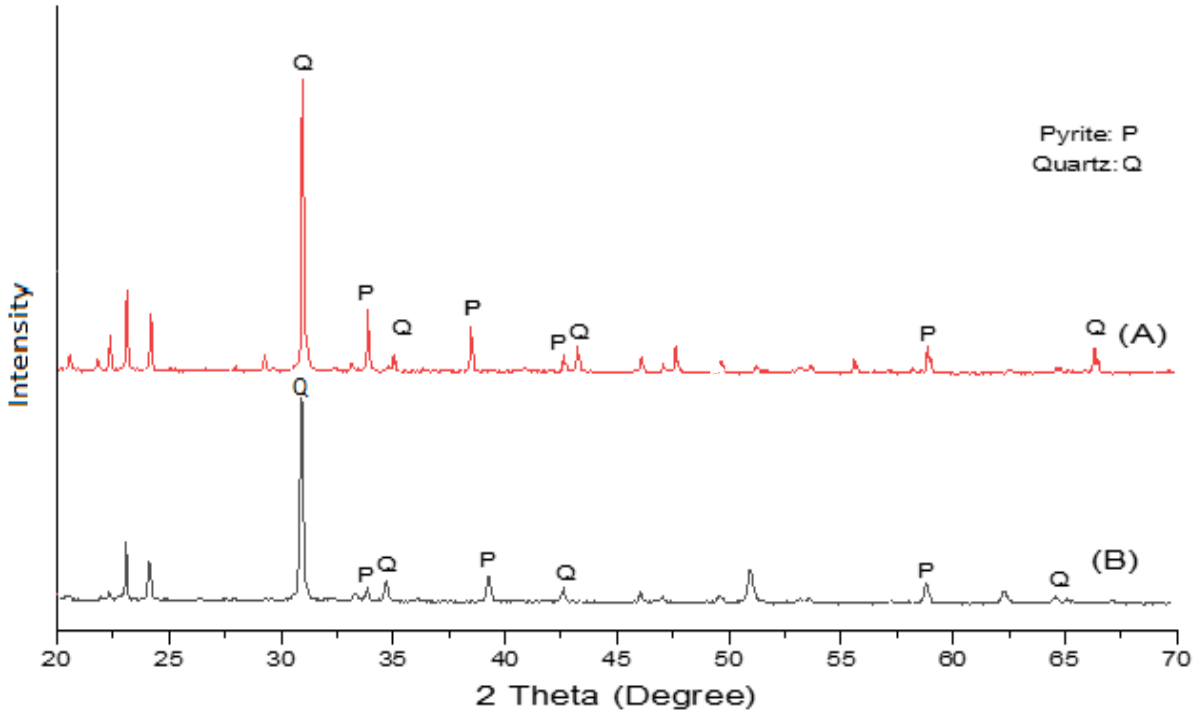

Figure 4. 16: X-ray diffractogram of the tailings (A) before gas-phase extraction and (B) after gas-phase extraction with acetylacetone

4.3.3 The gas-phase extraction of gold in tailings: A kinetic description

Many processes in metallurgical and materials engineering involve heterogeneous chemical reactions. As such they involve the transfer of species between phases (Seetharaman *et al.* 2014). Kinetics is the study of an aspect of these, indeed all, reactions—their mechanisms and rates and how conditions affect both. This section explores the kinetics of the gas-phase extraction of gold from tailings. The method used is statistical and inferential. It is based on two premises, (1) that a reaction curve—the extent of reaction with time—*manifests* the underlying mechanism, and (2) that the mechanism can be *inferred* by *matching* the reaction curve to a model and so transferring the elements of that model to the reaction under study. Such thinking has developed into a technique for determining the rate-limiting step of a heterogeneous reaction of two or more steps.

The first part of the technique is identifying the class of reaction. Machiba (2020) assumed the gas-phase extraction of gold from tailings—the very same reaction in

this study—to conform to a shrinking core. In this study the shrinking particle model is used for the following reasons:

1. The particles in tailings are gangue minerals, mostly quartz (see Table 3.3). Grains of gold are associated with these particles as inclusions (mostly) in pyrite (FeS_2), inclusions exhibiting varying degrees of liberation. Gold, in other words, is a *fragment* of a *very small fraction* of particles.
2. The reaction between gold and ligand is topochemical; the reaction leaves no solid product behind on the residue. There is, in other words, no solid product layer—porous or not—through which gaseous or ionic reactants or products must diffuse. Thus, there is no shrinking core.
3. Organic ligand, one of the reactants, reaching the surface of a grain of gold, reacts with gold exposed at the surface. As it does so, the reaction surface recedes to the centre of the grain; the grain shrinks. This class of reaction would be better described as a shrinking sphere. But even this description is somewhat off the mark: (1) gold grains that are partially liberated will react with ligand over only a fraction of gold interface, the free surface, and (2) gold grains locked in pyrite remain shielded from ligand until all of the pyrite encasing it is consumed.

Levenspiel (1999) describes three potential rate-limiting steps in this class of reaction. That description can be applied to the reaction with gold (see reaction 4.6): (1) ligand diffuses from the main body of the gas through a boundary-layer film at the surface of gold, (2) gold and the ligand react at the surface, and (3) the organometallic product diffuses through the boundary layer and into the main body of the gas flowing through the bed of particles.

$$\text{Ligand(g)} + b\text{Au(s)} \rightarrow \text{Organometallic product(g)} \qquad [4.6a]$$

or, more generally,

$$\text{A(g)} + b\text{B(s)} \rightarrow \text{Product} \qquad [4.6b]$$

In this analysis, one of these steps is assumed to be rate limiting—either chemical reaction (step 2) or diffusion (step 1 or step 3).

In chemical-reaction control, the resistance is due solely to the chemical reaction and the rate of the solid disappearance is directly related to the surface area of gold exposed (Kunii and Levenspiel, 1991; see Equation 4.7):

$$-\frac{1}{4\pi r_c^2}\frac{dN_A}{dt} = -\frac{1}{4\pi r_c^2 b}\frac{dN_B}{dt} = k_c C_A \qquad [4.7]$$

k_c is the rate constant of the reaction and it is directly related to the volume fraction of B in the solid (Kunii and Levenspiel, 1991). The extent of the reaction in terms of the radius of the sphere (r_c) or conversion X_B is;

$$\frac{t}{\tau} = 1 - \frac{r_c}{R} = 1 - (1 - X_B)^{1/3} \qquad [4.8]$$

where X_B is the fraction of gold extracted at time (t).

The time required to completely convert an unreacted particle into a product is

$$\tau = \frac{\rho_B R}{b k_c C_A} = \frac{\rho_B d_p}{2 b k_c C_A} \qquad [4.9]$$

where ρ_B is the density of the solid B and b is the stoichiometric coefficient of B.

In gas-solid chemical reactions where the activated complex forms rapidly the reaction rate is most likely controlled by diffusion. Diffusion control means that the rate at which gas is supplied to the solid surface is controlled by diffusion through an external boundary layer. The progress for a diffusion controlled reaction is shown in Equation 4.10.

$$\frac{t}{\tau} = 1 - (1 - X_B)^{2/3} \qquad [4.10]$$

where $\tau = \frac{\rho_B R^2}{2 b D_s C_A}$ [4.11]

and D_s is the effective diffusivity of the gas reactant A.

The kinetics of the gas-phase extraction process with acetylacetone was studied using a shrinking-sphere model to determine the rate-limiting step in the process. The results at intervals (30, 60, 120, 180 min) at different temperatures (190, 210, and 250°C) were plotted in terms of Equation 4.8 (chemical-reaction control) and Equation 4.10 (diffusion controlled) of the shrinking-sphere model. Figures 4.17 and 4.18 show the

data plotted for chemical reaction controlled and the diffusion controlled kinetic models for the gas-phase extraction, respectively.

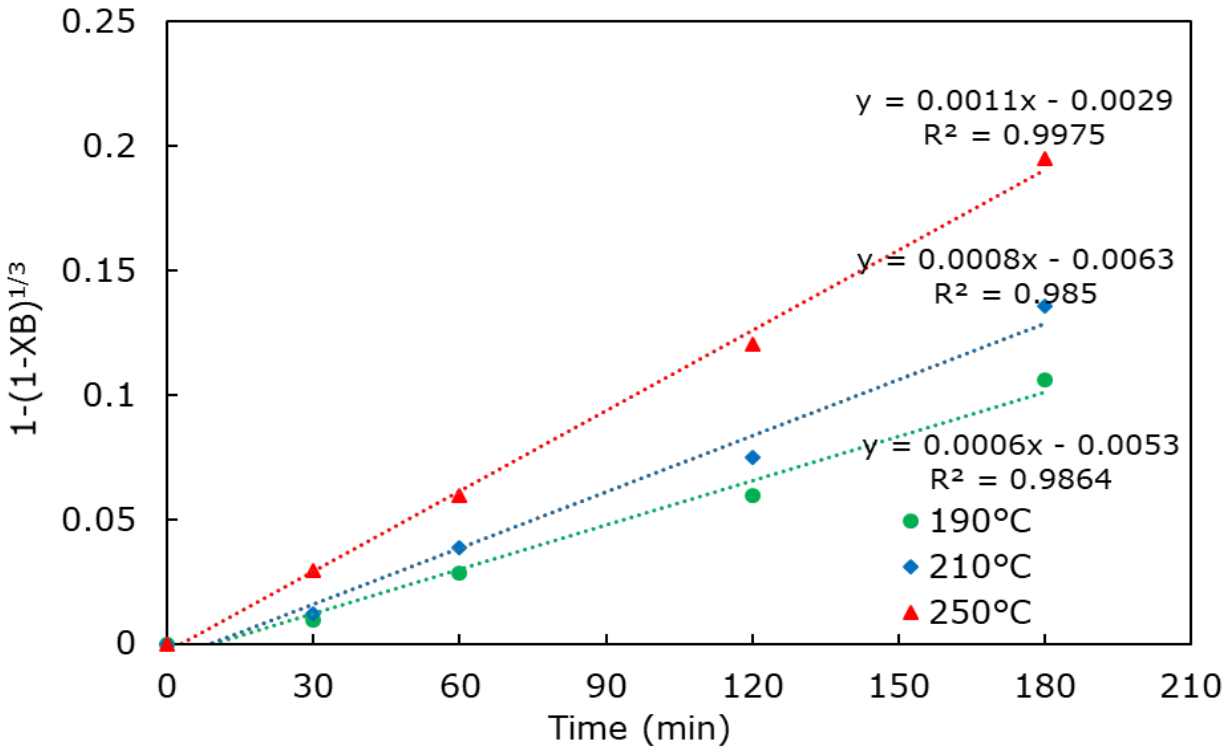

Figure 4.17: Shrinking-sphere, chemical-reaction control plot of the gas-phase extraction of gold at different temperatures

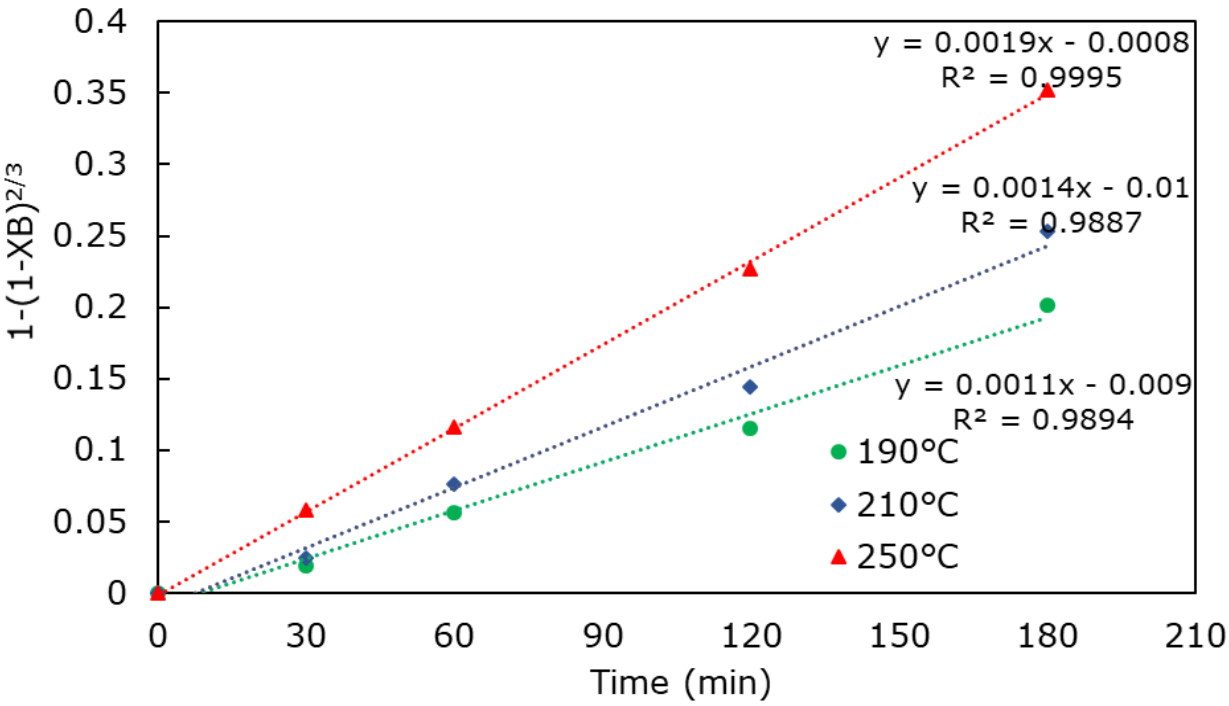

Figure 4.18: Shrinking-sphere, diffusion control of the gas-phase extraction of gold at different temperatures

One might infer from the R^2 values in Figures 4.17 and 4.18 that the gas-phase extraction of gold from the tailings is diffusion controlled rather than chemical-reaction controlled, as the R^2 values are closer to one in Figure 4.18 than Figure 4.17. One might just as easily conclude that the evaluation is either inconclusive or controlled roughly equally by both steps. As diffusion-control edges out chemical-reaction control in the statistical count, I carry it forward in evaluating the activation energy, which is governed by the Arrhenius equation:

$$k = Ae^{\frac{E_a}{RT}} \qquad [4.12]$$

where A is a pre-exponential factor, E_a is the activation energy, R is the universal gas constant (8.3145 J/[mol·K]) and T is the temperature (K). The rate constant (k) was obtained from the slopes of the equations shown in Figure 4.18. The gradient of the plot of ln k against $1/T$ gives $-E_a/RT$.

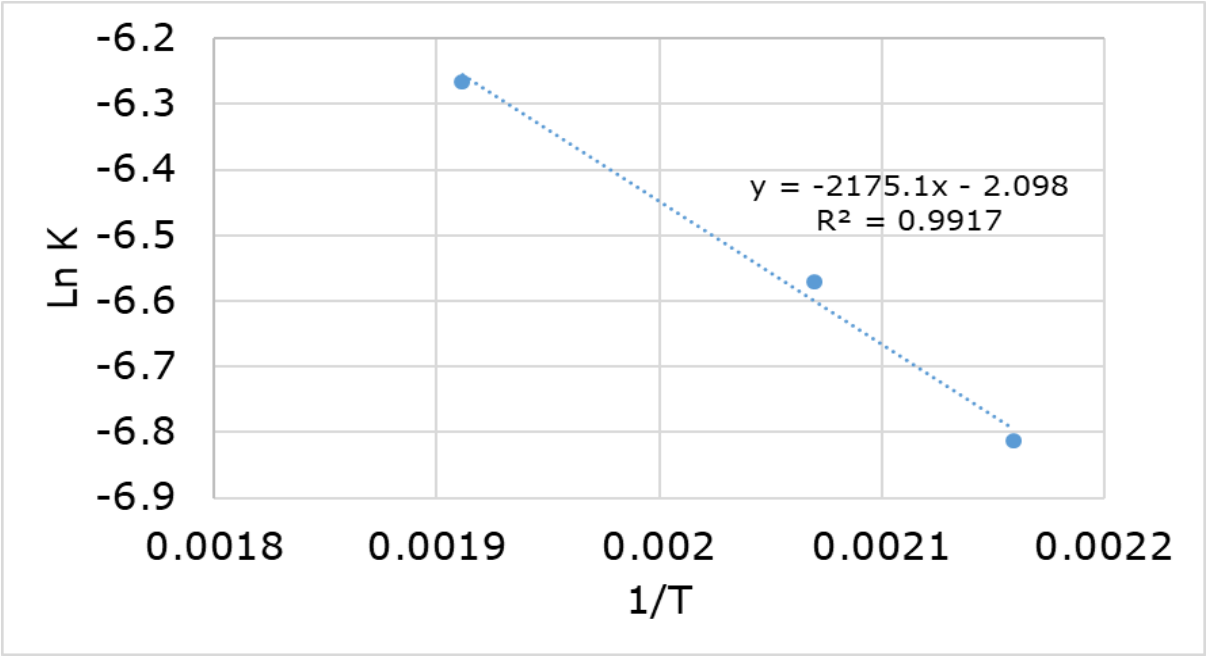

Figure 4.19: Arrhenius plot for the gas phase extraction of gold at different temperatures

From the slope of the graph (Figure 4.19) an activation energy of 18 kJ/mol was calculated (assuming the extent of extraction is proportional to time). Activation energy of <40 kJ/mol is indicative of a diffusion-reaction control (Uğuz and Geyikçi, 2019). One might infer diffusion as the rate-limiting step in this process. If diffusion were controlling, however, they it is unlikely to be through a thin boundary layer on free gold, but rather through the voids in a bed of tailings. These are much longer diffusion paths. Such control has not been modelled in this investigation. (The values of parameters in such a model would be difficult to determine.)

5 Conclusion and recommendation

5.1 Conclusion

This research investigated the feasibility of using gas-phase extraction to extract gold from a tailing material. In this section the outcomes of the objectives are discussed.

5.1.1 To determine physical properties and chemical composition of a typical low-grade ore and determine the fluidizability of this tailings material

The material has particle density (3.15 g/cm^3) and (Sauter) mean diameter (9 μm) and falls in group C of Geldart 's classification. At these fine sizes cohesive forces hold particles together tightly—so much so that these materials do not fluidize without extraordinary measures. A fluidized bed was therefore disqualified for this process and a fixed bed reactor was used as the mode of contact for the gas-phase extraction. It has its limitations in that the kinetics of extraction become an artefact of the experimental set-up.

5.1.2 To test selected β-diketonato ligands for the gas-phase extraction of gold

Literature study has shown that β-diketone ligands such as acetylacetone and its derivatives could be used as the volatile ligand in the gas-phase process. Acetylacetone was used as the extractant in the gas-phase extraction. The other potential β-diketone ligands for the gas-phase such as hexafluoroacetylacetone and trifluoroacetylacetone has not been investigated in this study, since our gas-phase set up requires large amount of the ligand and these ligands are expensive. However, the selectivity of the three ligands (Acetylacetone, hexafluoroacetylacetone and trifluoroacetylacetone) for the extraction of gold was examined in the liquid-phase system (not much ligand is needed in liquid-phase tests). Hexafluoroacetylacetone gave slightly higher yields of gold than either acetylacetone or trifluoroacetylacetone.

5.1.3 To measure the rate of gold extraction using acetylacetone

The extraction of gold was measured at temperatures of 190, 210, and 250°C and bed mass of 20 g. As expected, the highest extraction of gold was obtained at 250°C with extraction efficiency of 50%. This compares favourably with observations made by Van Dyk *et al.* (2012), extracting iron from iron ore fines, and Shemi *et al.* (2012), extracting aluminium from fly ash, in a gas phase with acetylacetone. These authors extracted the highest amount of the metal at 250°C extracting 80% of iron and 66% of Aluminum respectively. Furthermore, Machiba (2020) extracted gold from tailings using acetylacetone in a gas-phase, he extracted 65% of the gold at 250°C. The difference in extraction in Machiba's work and in this work could be due to the different reaction conditions. Machiba did not use compressed air in his system, compressed air was used in this current work and as such the partial pressure of the ligand could be a contributing factor. A possibility of which was not tested and should be investigated further.

5.1.4 To identify which of the Au (III) acetylacetonate complexes is most stable by DFT and also determine the relative stabilities of three Au(III)(β-diketonato)$_3$ complexes by DFT

The stabilities of $[Au(acac)_2]^-$ and $Au(acac)_3$ were assessed in the framework of DFT. Both $[Au(acac)_2]^-$ and $Au(acac)_3$ can exist under the correct reaction conditions. However, $Au(acac)_3$ complex is energetically favoured. Furthermore, DFT revealed that the $[Au(acac)_2]^-$ complex is square planar and the $Au(acac)_3$ is octahedral.

A DFT study on the structure and properties of three Au(III)- β-diketonato complexes was also carried out. The three complexes are Au(III) acetylacetonate, Au(III) trifluoroacetylacetonate, and Au(III) hexafluoroacetylacetonate. The HOMO-LUMO gaps of the Au(III)(β-diketonato)$_3$ complexes have been calculated and were found to be closely comparable, showing that the three complexes have similar stabilities. The findings were significant as these results can be used to predict the extraction potential

of these β-diketones. DFT shows that all three ligands will likely have similar extraction efficiencies in the gas-phase, and therefore just one ligand need be tested. The ligand chosen was acetylacetone because, compared with the other β-diketone ligands investigated, it is relatively cheap and less-toxic. For equal volumes of ligand, trifluoroacetylacetone is almost 45 times more expensive and hexafluoroacetylacetone 90 times more expensive than acetylacetone.

5.1.5 To determine the kinetics of the gas-phase extraction process

The kinetics of the gas-phase extraction process with acetylacetone was modelled on a shrinking sphere. To determine the rate-limiting step in the process, the gas-phase extraction results at intervals—30, 60, 120, 180 min—at different temperatures—190, 210, and 250°C—were tested against chemical-reaction-control and diffusion-control models. Although the correlation coefficients (R^2) of both tests were similar, diffusion control gave a slightly higher correlation. Diffusion control was inferred. But the inference is tentative at best, for the statistics underlying the inference, given the uncertainties of measurement, is unable to resolve satisfactorily differences in correlations, and the logic of inference is open ended.

An activation energy of 18 kJ/mol was calculated. A low activation energy is indicative of diffusion control.

5.1.6 To test the stability of pyrite

The SEM images of the solid residue after the gas-phase extraction showed a decrease in pyrite particles. Additionally, an XRD diffractogram of the tailings after the gas-phase extraction showed a significant decrease in the intensity of the pyrite peaks further indicating that the acetylacetone ligand breaks down the pyrite during gas-phase extraction and as such should release more of the locked gold.

5.2 Recommendations

The following recommendations are made based on the understanding gained during this study.

- Doing the gas-phase extraction in a fluidized bed should be considered, as handling of solids is easy and mass and heat transfer rates are good in fluidized beds. As the fine particles cohere, one might consider micro-granulation.
- The use of Schiff Bases (nitrogen equivalent of an aldehyde) as the ligands in this process should be considered.

References

Aihara, J. (1999). Reduced HOMO−LUMO Gap as an Index of Kinetic Stability for Polycyclic Aromatic Hydrocarbons. *The Journal of Physical Chemistry A*, 103(37), 7487–7495. doi:10.1021/jp990092i

Ajbar, A., Bakhbakhi, Y., Ali, S., and Asif, M. (2011). Fluidization of Nano-Powders: Effect of Sound Vibration and Pre-Mixing with Group A Particles. *Powder Technology* 206 (3): 327–37. https://doi.org/10.1016/j.powtec.2010.09.038.

Allimann-Lecourt, C., Bailey, T. H., and Cox, M. (2002). Purification of combustion fly ashes using the SERVO process. *Journal of Chemical Technology and Biotechnology*, 77(3), pp. 260–266. doi: 10.1002/jctb.548.

Atkins, P., and De Paula, J. (2010). *Atkins' Physical chemistry*. 9th ed. Oxford: Oxford University Press.

Bai, Y., and Yang, H. J. (2006). Metal ion extraction using newly-synthesized bipyridine derivative as a chelating reagent in supercritical CO 2. *Analytical Sciences*, 22(11), pp. 1469–1471. doi: 10.2116/analsci.22.1469.

Becke, A. D. A New Mixing of Hartree–Fock and Local Density-Functional Theories. *The Journal of Physical Chemistry A* (1993), *98*, 1372–1377.

La Brooy, S. R., Linge, H. G., and Walker, G. S. (1994). Review of gold extraction from ores. *Minerals Engineering*, 7(10), pp. 1213–1241. doi: 10.1016/0892-6875(94)90114-7.

Chen, Y., Mariba, E. R.M., Van Dyk, L., and Potgieter, J. H. (2011). A Review of Non-Conventional Metals Extracting Technologies from Ore and Waste. *International Journal of Mineral Processing* 98 (1–2): 1–7. https://doi.org/10.1016/j.minpro.2010.10.001.

Coetzee, L.L., Salomon J.T., Gavin J.M., Van Der Merwe J.D., and Stanek, T.A. (2011). Modern Gold Deportments and Its Application to Industry. *Minerals Engineering* 24 (6): 565–75. https://doi.org/10.1016/j.mineng.2010.09.001.

Conradie, J., Mateyise, N. G. S., and Conradie, M. M. (2019). Reduction Potential of β-diketones: effect of electron donating, aromatic and ester groups. *South African Journal of Science and Technology*, 38(1), p. 1. Available at: http://www.satnt.ac.za/index.php/satnt/article/view/727.

Conradie, M. M., and Conradie, J. (2015b). Electrochemical behaviour of Tris(β-diketonato)iron(III) complexes: A DFT and experimental study. *Electrochimica Acta*, 152, pp. 512–519. doi: 10.1016/j.electacta.2014.11.128.

DRDGOLD (2017) Annual integreated report 2017. DRDGOLD Limited, Johannesburg.

Dworzanowski, M. (2018). A mineralogical investigation into the nature and deportment of gold in ERGO flotation feed and concentrate, Johannesburg: University of the Witwatersrand

M.J. Frisch, G.W. Trucks, H.B. Schlegel, G.E. Scuseria, M.A. Robb, J.R. Cheeseman, G. Scalmani, V. Barone, B. Mennucci, G.A. Petersson, H. Nakatsuji, M. Caricato, X. Li, H.P. Hratchian, A.F. Izmaylov, J. Bloino, G. Zheng, J.L. Sonnenberg, M. Hada, M. Ehara, K. Toyota, R. Fukuda, J. Hasegawa, M. Ishida, T. Nakajima, Y. Honda, O. Kitao, H. Nakai, T. Vreven, J.A. Montgomery (Jr.), J.E. Peralta, F. Ogliaro, M. Bearpark, J.J. Heyd, E. Brothers, K.N. Kudin, V.N. Staroverov, R. Kobayashi, J. Normand, K. Raghavachari, A. Rendell, J.C. Burant, S.S. Iyengar, J. Tomasi, M. Cossi, N. Rega, J.M. Millam, M. Klene, J.E. Knox, J.B. Cross, V. Bakken, C. Adamo, J. Jaramillo, R. Gomperts, R.E. Stratmann, O. Yazyev, A.J. Austin, R. Cammi, C. Pomelli, J.W. Ochterski, R.L. Martin, K. Morokuma, V.G. Zakrzewski, G.A. Voth, P. Salvador, J.J. Dannenberg, S. Dapprich, A.D. Daniels, Ö. Farkas, J.B. Foresman, J.V. Ortiz, J. Cioslowski, D.J. Fox, Gaussian 09, Revision D.01, Gaussian, Inc., Wallingford, CT (2009).

Fuentealba, P., Preuss, H., Stoll, H. and Szentpály, L. v. (1982). A Proper Account of Core-polarization with Pseudopotentials – Single Valence-Electron Alkali Compounds. *The Journal of Physical Chemistry A*., 89, 418-22. DOI: 10.1016/0009-2614(82)80012-2

Qi, S. C., Hayashi, J. I. and Zhang, L. (2016). Recent application of calculations of metal complexes based on density functional theory', *RSC Advances*, 6(81), pp. 77375–77395. doi: 10.1039/c6ra16168e.

Fukui, K., Yonezawa, T., and Shingu, H. (1952). A molecular orbital theory of reactivity in aromatic hydrocarbons. *The Journal of Chemical Physics*, 20(4), pp. 722–725. doi: 10.1063/1.1700523.

Geldart, D. (1973). Types of Gas Fluidization. 7, pp. 285–292.

Gupta, C. K., and Mukherjee, T. K. (1990). *Hydrometallurgy in extraction processes Volume II*. doi: 10.1201/9780203751428.

Haas, K., and Franz, K. (2009). Application of Metal Coordination Chemistry to Explore and Manipulate Cell Biology. *Chemical Reviews*, 109(10), pp.4921-4960.

Habashi, F. (1967). Kinetics and mechanism of gold and silver dissolution in cyanide solution', *PhD*, Montana college of mineral science and technology.

Han, M. (2015). Characterization of fine particle fluidization', (August), p. 101.

Hilson, G., and Monhemius, A. J. (2006). Alternatives to cyanide in the gold mining industry: what prospects for the future?. *Journal of Cleaner Production*, 14(12-13 SPEC. ISS.), pp. 1158–1167. doi: 10.1016/j.jclepro.2004.09.005.

Ivankovits, J. C., (2000). Reactions of hexafluoroacetylacetone with selected metal oxides, metal films, and metallic contaminants on copper, tin-lead solder, and silicon surfaces. MSc dissertation, Lehigh university

JS.Ogola, T.Shavhani., R. M. (2018). Possibilities of Reprocessing Tailings Dams for Gold and other Minerals: A Case Study of South Africa. *Journal of Environmental Science and Allied Research*, pp. 39–42. doi: 10.29199/esar.101016.

Kunii, D., & Levenspiel, O. (1991). *Fluidization Engineering*. 2nd edition. Butterworth-Heinemann, USA

Laboureur, L., Ollero, M., and Touboul, D. (2015). Lipidomics by supercritical fluid chromatography. *International Journal of Molecular Sciences*, 16(6), pp. 13868–13884. doi: 10.3390/ijms160613868.

Leion, H., Frick, V., and Hildor, F. (2018). Experimental Method and Setup for Laboratory Fluidized Bed Reactor Testing. doi: 10.3390/en11102505.

Levenspiel, O. (1999). *Chemical reaction engineering*. 3rd ed. Portland: John Wiley & Sons, pp.577-580.

Leybros, A., Agnès G., Nathalie S., Marc M., and Olivier B. (2016). Cesium Removal from Contaminated Sand by Supercritical CO2 Extraction. *Journal of Environmental Chemical Engineering* 4 (1): 1076–80. https://doi.org/10.1016/j.jece.2016.01.009.

Machiba, Muofhe Darlington. (2020). Gold Recovery in a Fluidized Bed with a Gas Phase Extractant. MSc dissertation, University of the Witwatersrand

Marsden, J., and House, I. (2006). The chemistry of gold extraction. 2nd ed. Littleton, Colo.: Society for Mining, Metallurgy, and Exploration, pp.1-3.

Mawire, Godfrey Takudzwa. (2019). Supercritical Extraction of Gold from Refractory Ores. MSc dissertation, University of the Witwatersrand

Mbayo, J. J. K., Simonsen, H., and Ndlovu, S. (2019). Improving the gold leaching process of refractory ores using the Jetleach reactor. *Minerals Engineering*, 134(February), pp. 300–308. doi: 10.1016/j.mineng.2019.02.003.

Minerals Council South Africa (2018) 'Facts and Figures Pocket Book 2018', (June).

Mochizuki, Shunsuke., Naozumi Wada., Richard L. Smith., and Hiroshi Inomata. (1999). Perfluorocarboxylic Acid Counter Ion Enhanced Extraction of Aqueous Alkali Metal Ions with Supercritical Carbon Dioxide. *Analyst* 124 (10): 1507–11. https://doi.org/10.1039/a904873a.

Mpana, N. R. (2012). The extraction of aluminium from fly ash using acetylacetone in gaseous phase. MSc dissertation, University of the Witwatersrand

Neingo, P. N., and Tholana, T. (2016). Trends in productivity in the South African gold mining industry. *Journal of the Southern African Institute of Mining and Metallurgy*, 116(3), pp. 283–290. doi: 10.17159/2411-9717/2016/v116n3a10.

Olehile, Obakeng Daniel (2017). Gas Phase Extraction Of Vanadium From Spent Vanadium Catalyst And Tantalum From Tantalum Oxide. MSc dissertation, University of the Witwatersrand

Pacek, A. W., and Nienow, A. W. (1990). Fluidisation of fine and very dense hardmetal powders. *Powder Technology*, 60(2), pp. 145–158. doi: 10.1016/0032-5910(90)80139-P.

Pettinari, C., and Santini, C., (2016). IR and Raman Spectroscopies of Inorganic, Coordination and Organometallic Compounds. *Encyclopedia of Spectroscopy and Spectrometry*, pp. 347–358. doi: 10.1016/b978-0-12-803224-4.00338-1.

Potgieter, J. H., Kabemba, M. A., Teodorovic, A., Potgieter-Vermaak, S. S., and Augustyn, W. G. (2006). An Investigation into the Feasibility of Recovering Valuable Metals from Solid Oxide Compounds by Gas Phase Extraction in a Fluidised Bed. *Minerals Engineering* 19 (2): 140–46. https://doi.org/10.1016/j.mineng.2005.08.002.

Qi, S. C., Hayashi, J. I., and Zhang, L. (2016). Recent application of calculations of metal complexes based on density functional theory, *RSC Advances*, 6(81), pp. 77375–77395. doi: 10.1039/c6ra16168e.

Raganati, F., Chirone, R. and Ammendola, P. (2018). Gas-solid fluidization of cohesive powders. *Chemical Engineering Research and Design*, 133, pp. 347–387. doi: 10.1016/j.cherd.2018.03.034.

Seetharaman, S., McLean, A., Guthrie, R., and Sridhar, S. (2014). *Treatise on process metallurgy*. 1st ed. Oxford: Elsevier, pp.39-40.

Shamsuddin, M. (2016). *Physical chemistry of metallurgical processes*. 1st ed. New Jersey: John Wiley & Sons, pp.423-424.

Shemi, A., Mpana, R., Ndlovu, S., van Dyk, L., Sibanda, V. and Seepe, L., 2012. Alternative techniques for extracting alumina from coal fly ash. *Minerals Engineering*, 34, pp.30-37.

Shriver, D., Weller, M., Overton, T., Rourke, J. and Armstrong, F., (2010). Inorganic chemistry. 5th ed. Oxford: OXFORD UNIVERSITY PRESS, p.251.

Stephens, P. J., Devlin, F. J., Chabalowski, C. F., Frisch, M. J. (1994). Ab Initio Calculation of Vibrational Absorption and Circular Dichroism Spectra Using Density Functional Force Fields, J. *Phys. Chem. 98*, 11623-11627.

Tayyari, S. F., H. Rahemi, A. R., Nekoei, M., Zahedi-Tabrizi., and Y. A. Wang. (2007). Vibrational Assignment and Structure of Dibenzoylmethane. A Density Functional Theoretical Study. *Spectrochimica Acta - Part A: Molecular and Biomolecular Spectroscopy* 66 (2): 394–404. https://doi.org/10.1016/j.saa.2006.03.010.

Tshofu, G. S. (2014). Green Extraction Technology for the Extraction of Iron From Iron Ore Fines. MSc dissertation, University of the Witwatersrand

Turner, C., Eskilsson, C. S., and Björklund, E. (2002). Collection in analytical-scale supercritical fluid extraction. *Journal of Chromatography A*, 947(1), pp. 1–22. doi: 10.1016/S0021-9673(01)01592-8.

Uğuz, G. and Geyikçi, F. (2019). Kinetic Study on Copper Leaching in Electroplating Waste Sludge Using Ammonium Nitrate Solution. *Journal of Engineering and Sciences,* 5 (1): 1–15.

Van Dyk, L., Mariba, E., Chen, Y., and Potgieter, J.H. (2010). Gas phase extraction of iron from its oxide in a fluidized bed reactor. *Minerals Engineering,* 23(1), pp.58-60.

Van Rensburg, S. J. (2016). Guidelines for Retreatment of SA gold tailings: MINTEK's learnings. *Proceedings of the 23rd WasteCon Conference 17-21 October 2016, Emperors Palace, Johannesburg, South Africa*, (October), pp. 367–376.

Wai, W., Leong, E. and Mujumdar, A. S. (2009). Gold Extraction and Recovery Processes. *National University of Singapore*, pp. 5–10.

Wallen, S. L., C. R. Yonker, C. L. Phelps, and C. M. Wai. (1997). Effect of Fluorine Substitution, Pressure and Temperature on the Tautomeric Equilibria of Acetylacetonate β-Diketones. *Journal of the Chemical Society - Faraday Transactions* 93 (14): 2391–94. https://doi.org/10.1039/a701851g.

Xavier, A. and Srividhya, N., 2014. Synthesis and Study of Schiff base Ligands. *IOSR Journal of Applied Chemistry*, 7(11), pp.06-15.

Zawadiak, J., and Mrzyczek, M. (2012). Influence of substituent on UV absorption and keto-enol tautomerism equilibrium of dibenzoylmethane derivatives. *Spectrochimica Acta - Part A: Molecular and Biomolecular Spectroscopy*, 96, pp. 815–819. doi: 10.1016/j.saa.2012.07.109.

Zhou, J. Y., and Cabri, L. J. (2004). Gold process mineralogy: Objectives, techniques, and applications. *The Journal of The Minerals, Metals & Materials Society*, 56(7), pp. 49–52. doi: 10.1007/s11837-004-0093-7.

Appendix A: Calculation of extractions

Atomic absorption spectroscopy was used to determine the gold content in the tailings. Initial gold content of the tailing was determined by digesting 1 g of the sample in 20 ml of aqua regia. After each experiment the extraction liquor was collected and the gold content in that liquor was determined. The concentration can be represented by equation A-1.

$$C_{Au} = \frac{m_{Au}}{V_c} \qquad \text{[A-1]}$$

Where m_{Au} is the mass of the gold, C_{Au} is the concentration of the gold and V_c is the collected volume after extraction. The percentage of gold extracted was calculated using the equation below.

$$Percentage\ of\ gold\ extracted\ (\%) = \frac{m_{Au}\ extracted}{m_{Au}\ in\ the\ feed} \times 100 \qquad \text{[A-2]}$$

The sample was collected after every 30 minutes for the first hour, for the subsequent hours the sample was collected hourly. The Experimental results discussed in chapter 4 is represented in the following tables below.

Effect of temperature

Table A-1: Percentage of gold extracted at 3ml/min flowrate and temperature of 190 °C for a bed mass of 20 g.

Time (min)	Volume collected (L)	Concentration (mg/l)	Mass Au Extracted (mg)	Cummulative mass (mg)	Cummulative extraction of Gold (%)
0	0	0	0	0	0
30	0.026	0.09	0.00234	0.00234	2.93
60	0.03	0.144	0.00432	0.00666	8.33
120	0.034	0.2	0.0068	0.01346	16.82
180	0.041	0.23	0.00943	0.02289	28.61
240	0.03	0.03	0.0009	0.02379	29.74

Table A-2: Percentage of gold extracted at 3ml/min flowrate and temperature of 210 °C for a bed mass of 20 g.

Time (min)	Concentration (mg/l)	Volume collected (L)	Mass Au Extracted (mg)	Cummulative mass (mg)	Cummulative extraction of Gold (%)
0	0	0	0	0	0
30	0.1	0.029	0.0029	0.0029	3.63
60	0.19	0.032	0.00608	0.00898	11.23
120	0.22	0.035	0.0077	0.01668	20.85
180	0.243	0.048	0.011664	0.028344	35.43
240	0.03	0.033	0.00099	0.029334	36.67

Table A-3: Percentage of gold extracted at 3ml/min flowrate and temperature of 250 °C for a bed mass of 20 g.

Time (min)	Volume collected (L)	Concentration (mg/l)	Mass Au Extracted (mg)	Cummulative mass (mg)	Cummulative extraction of Gold (%)
0	0	0	0	0	0
30	0.043	0.12	0.00516	0.00688	8.6
60	0.039	0.17	0.00663	0.01351	16.89
120	0.053	0.228	0.012084	0.025594	31.99
180	0.055	0.23	0.01265	0.038244	47.81
240	0.038	0.04	0.00152	0.039764	49.71

Bed weight

Table A-4: Percentage of gold extracted at 3ml/min flowrate and temperature of 210 °C for a bed mass of 10 g.

Time (min)	Concentration (mg/l)	Volume collected (L)	Mass Au Extracted (mg)	Cummulative mass (mg)	Cummulative extraction of Gold (%)
0	0	0	0	0	0
30	0.15	0.032	0.0048	0.0048	6
60	0.2	0.035	0.007	0.0118	14.75
120	0.21	0.046	0.00966	0.02146	26.83
180	0.26	0.05	0.013	0.03446	43.08
240	0.04	0.031	0.00124	0.0357	44.63

Table A-5: Percentage of gold extracted at 3ml/min flowrate and temperature of 210 °C for a bed mass of 10 g

Time (min)	Concentration (mg/l)	Volume collected (L)	Mass Au Extracted (mg)	Cummulative mass (mg)	Cummulative extraction of Gold
0	0	0	0	0	0
30	0.1	0.029	0.0029	0.0029	3.63
60	0.19	0.032	0.00608	0.00898	11.23
120	0.22	0.035	0.0077	0.01668	20.85
180	0.243	0.048	0.011664	0.028344	35.43
240	0.03	0.033	0.00099	0.029334	36.67

Appendix B: Kinetic data

Table B1: data for shrinking sphere diffusion control of the gas-phase extraction of gold at different temperatures

Time (min)	X_B 190°C	X_B @ 210°C	X_B @ 250°C	$1-(1-XB)^{2/3}$ @ 190°C	$1-(1-XB)^{2/3}$ @ 210°C	$1-(1-XB)^{2/3}$ @ 250°C
0	0	0	0	0	0	0
30	0.02925	0.03625	0.086	0.01959632	0.024315077	0.058188
60	0.08325	0.11225	0.168875	0.05630002	0.076308131	0.116016
120	0.16825	0.2085	0.319925	0.115573243	0.144341217	0.226659
180	0.286125	0.3543	0.47805	0.201242807	0.252942797	0.351735
240	0.297375	0.366675	0.49705	0.20965678	0.262518572	0.367564

Table B2:data for shrinking sphere chemical reaction control of the gas-phase extraction of gold at different temperatures

Time (min)	X_B @ 190°C	X_B @ 210°C	X_B @ 250°C	$1-(1-X_B)^{1/3}$ @ 190°C	$1-(1-X_B)^{1/3}$ @ 210°C	$1-(1-XB)^{1/3}$ @ 250°C
0	0	0	0	0	0	0
30	0.02925	0.03625	0.086	0.009846638	0.012232	0.02953
60	0.08325	0.11225	0.168875	0.028557784	0.038911	0.059796
120	0.16825	0.2085	0.319925	0.059560338	0.074982	0.120602
180	0.286125	0.3543	0.47805	0.106267829	0.135675	0.194851
240	0.297375	0.366675	0.49705	0.110987503	0.141233	0.204742

Appendix C: Density functional theory data

Optimized Cartesian coordinates (Å) of the Au(III)- *β*-diketonato complexes.

The Au β-diketonato complexes were optimized using the Gaussian 16 package. The B3LYP functional and the Stuttgart/Dresden (SDD) basis set were used for all atoms.

Au(III) acetylacetonate- (a) $Au(acac)_3$

C	0.945618000000	1.875115000000	–2.069888000000
O	1.176399000000	0.805042000000	–1.288980000000
Au	0.000000000000	0.000000000000	0.156383000000
O	–1.188310000000	2.393499000000	0.093601000000
C	–1.014182000000	3.109160000000	–0.942363000000
C	0.000000000000	2.882168000000	–1.960480000000
H	0.029705000000	3.625752000000	–2.751842000000
C	1.949456000000	1.893962000000	–3.213291000000
H	1.821128000000	2.777034000000	–3.845988000000
H	1.834283000000	0.988707000000	–3.822424000000
H	2.967951000000	1.884998000000	–2.806194000000
H	–2.605746000000	4.421167000000	–0.317481000000
H	–1.317913000000	5.241374000000	–1.250136000000
C	–1.915213000000	4.324156000000	–1.159305000000
H	–2.490715000000	4.212064000000	–2.088425000000
C	1.014182000000	–3.109160000000	–0.942363000000
O	1.188310000000	–2.393499000000	0.093601000000
O	–1.176399000000	–0.805042000000	–1.288980000000
C	–0.945618000000	–1.875115000000	–2.069888000000
C	0.000000000000	–2.882168000000	–1.960480000000
H	–0.029705000000	–3.625752000000	–2.751842000000
C	1.915213000000	–4.324156000000	–1.159305000000
H	2.605746000000	–4.421167000000	–0.317481000000

H	2.490715000000	–4.212064000000	–2.088425000000
H	1.317913000000	–5.241374000000	–1.250136000000
H	–1.821128000000	–2.777034000000	–3.845988000000
H	–2.967951000000	–1.884998000000	–2.806194000000
C	–1.949456000000	–1.893962000000	–3.213291000000
H	–1.834283000000	–0.988707000000	–3.822424000000
C	0.990593000000	0.781520000000	2.866143000000
O	1.172386000000	0.910336000000	1.573233000000
O	–1.172386000000	–0.910336000000	1.573233000000
C	–0.990593000000	–0.781520000000	2.866143000000
C	0.000000000000	0.000000000000	3.499242000000
H	0.000000000000	0.000000000000	4.581759000000
C	1.979269000000	1.579028000000	3.689559000000
H	1.836492000000	1.422271000000	4.761731000000
H	1.864203000000	2.645428000000	3.459623000000
H	3.000504000000	1.294100000000	3.410332000000
H	–1.836492000000	–1.422271000000	4.761731000000
H	–3.000504000000	–1.294100000000	3.410332000000
C	–1.979269000000	–1.579028000000	3.689559000000
H	–1.864203000000	–2.645428000000	3.459623000000

Au(III) acetylacetone–(b) $[Au(acac)_2]^+$

Au	0.000000000000	0.000000000000	0.000000000000
O	1.395896000000	1.465772000000	0.000000000000
O	–1.395896000000	–1.465772000000	0.000000000000
O	–1.395896000000	1.465772000000	0.000000000000
O	1.395896000000	–1.465772000000	0.000000000000
C	–2.705863000000	1.258134000000	0.000000000000
C	–3.338209000000	0.000000000000	0.000000000000
C	–2.705863000000	–1.258134000000	0.000000000000
C	–3.514092000000	–2.533743000000	0.000000000000
C	–3.514092000000	2.533743000000	0.000000000000
C	2.705863000000	1.258134000000	0.000000000000
C	3.338209000000	0.000000000000	0.000000000000
C	2.705863000000	–1.258134000000	0.000000000000
C	3.514092000000	2.533743000000	0.000000000000
C	3.514092000000	–2.533743000000	0.000000000000
H	4.421925000000	0.000000000000	0.000000000000
H	–4.421925000000	0.000000000000	0.000000000000
H	–4.161015000000	2.570145000000	0.885416000000
H	–2.854282000000	3.403102000000	0.000000000000
H	–4.161015000000	2.570145000000	–0.885416000000
H	–4.161015000000	–2.570145000000	0.885416000000
H	–4.161015000000	–2.570145000000	–0.885416000000
H	–2.854282000000	–3.403102000000	0.000000000000
H	2.854282000000	–3.403102000000	0.000000000000
H	4.161015000000	–2.570145000000	0.885416000000
H	4.161015000000	–2.570145000000	–0.885416000000
H	4.161015000000	2.570145000000	–0.885416000000
H	4.161015000000	2.570145000000	0.885416000000
H	2.854282000000	3.403102000000	0.000000000000

Au(III) trifluoroacetylacetone– $Au(tfa)_3$

C	2.377589000000	–1.165339000000	–1.270167000000
O	1.532660000000	–0.131394000000	–1.363280000000
Au	–0.190843000000	0.234667000000	–0.366133000000
O	0.081105000000	–2.255085000000	0.520435000000
C	1.158293000000	–2.840201000000	0.211583000000
C	2.245682000000	–2.377024000000	–0.593220000000
H	3.087446000000	–3.050606000000	–0.689810000000
C	3.643575000000	–0.875212000000	–2.054229000000
H	4.267528000000	–1.767439000000	–2.149513000000
H	4.213742000000	–0.093470000000	–1.536113000000
H	3.387853000000	–0.496320000000	–3.049896000000
C	1.290016000000	–4.295833000000	0.752620000000
C	0.494484000000	3.568328000000	–1.213447000000
O	–0.472726000000	2.763067000000	–1.330144000000
O	0.883425000000	1.347808000000	0.957155000000
C	1.733589000000	2.326058000000	0.617449000000
C	1.620353000000	3.344937000000	–0.292455000000
H	2.435650000000	4.058486000000	–0.340604000000
C	0.541850000000	4.842600000000	–2.038859000000
H	0.580692000000	5.722780000000	–1.382954000000
H	–0.343115000000	4.904468000000	–2.676416000000
H	1.444987000000	4.861985000000	–2.664118000000
C	3.009395000000	2.224813000000	1.461775000000
C	–2.518977000000	–1.201017000000	–1.612906000000
O	–1.248159000000	–0.918330000000	–1.710534000000
O	–1.891568000000	0.717818000000	0.673032000000
C	–3.057902000000	0.209977000000	0.377835000000
C	–3.411568000000	–0.678012000000	–0.635234000000
H	–4.444945000000	–0.991314000000	–0.691407000000
C	–3.020500000000	–2.182334000000	–2.644502000000

H	–4.097027000000	–2.082586000000	–2.806662000000
H	–2.815174000000	–3.202094000000	–2.289145000000
H	–2.482708000000	–2.044732000000	–3.586810000000
C	–4.148690000000	0.727058000000	1.333167000000
F	0.875988000000	–4.399807000000	2.075399000000
F	2.594203000000	–4.810644000000	0.691337000000
F	0.484730000000	–5.167522000000	–0.003490000000
F	2.745023000000	2.148991000000	2.826385000000
F	3.740621000000	1.068966000000	1.123114000000
F	3.880226000000	3.307572000000	1.276453000000
F	–4.297255000000	2.109679000000	1.222870000000
F	–3.843473000000	0.437522000000	2.659424000000
F	–5.399995000000	0.158390000000	1.063864000000

Au(III) hexafluoro–acetylacetone– $Au(hfa)_3$

C	1.597951000000	1.031454000000	–1.998219000000
O	1.430320000000	0.090665000000	–1.063795000000
Au	0.000000000000	0.000000000000	0.367116000000
O	0.381831000000	2.657613000000	0.212123000000
C	0.756216000000	3.116213000000	–0.893465000000
C	1.336579000000	2.379674000000	–1.997624000000
H	1.583881000000	2.933982000000	–2.895022000000
C	2.243152000000	0.392774000000	–3.239995000000
C	0.622444000000	4.646070000000	–1.138148000000
C	–0.756216000000	–3.116213000000	–0.893465000000
O	–0.381831000000	–2.657613000000	0.212123000000
O	–1.430320000000	–0.090665000000	–1.063795000000
C	–1.597951000000	–1.031454000000	–1.998219000000
C	–1.336579000000	–2.379674000000	–1.997624000000
H	–1.583881000000	–2.933982000000	–2.895022000000
C	–0.622444000000	–4.646070000000	–1.138148000000
C	–2.243152000000	–0.392774000000	–3.239995000000
C	1.223781000000	0.158458000000	3.083254000000
O	1.459815000000	0.182788000000	1.806621000000
O	–1.459815000000	–0.182788000000	1.806621000000
C	–1.223781000000	–0.158458000000	3.083254000000
C	0.000000000000	0.000000000000	3.751596000000
H	0.000000000000	0.000000000000	4.832701000000
C	2.516715000000	0.328540000000	3.909631000000
C	–2.516715000000	–0.328540000000	3.909631000000
F	0.000000000000	5.299517000000	–0.094326000000
F	–0.109507000000	4.901455000000	–2.306450000000
F	1.888643000000	5.224676000000	–1.316655000000
F	–3.484321000000	0.164904000000	–2.935313000000
F	–1.438427000000	0.635694000000	–3.743479000000

F	–2.441369000000	–1.307970000000	–4.272115000000
F	–3.141572000000	–1.531762000000	3.603470000000
F	–3.407872000000	0.705308000000	3.643556000000
F	–2.256794000000	–0.321916000000	5.280267000000
F	2.441369000000	1.307970000000	–4.272115000000
F	1.438427000000	–0.635694000000	–3.743479000000
F	3.484321000000	–0.164904000000	–2.935313000000
F	2.256794000000	0.321916000000	5.280267000000
F	3.141572000000	1.531762000000	3.603470000000
F	3.407872000000	–0.705308000000	3.643556000000
F	0.000000000000	–5.299517000000	–0.094326000000
F	–1.888643000000	–5.224676000000	–1.316655000000
F	0.109507000000	–4.901455000000	–2.306450000000